Assessment of Potential Commercial Success of Business Jets with Natural Laminar Flow

Stanislav Karpuk *
Technical University Braunschweig, Braunschweig, Germany

Ali Elham†
University of Southampton, Southampton, United Kingdom

The present research investigates the potential application of the Natural Laminar Flow wing technology to business jet market segments from light to long-range jets. A database of existing business jets was generated to determine the range extension as a potential driver of customer interest. A conceptual design of several configurations for each market segment was performed to investigate potential improvements in the aircraft flight range, operating costs, and price changes using the technology. An initial sizing module and a low-fidelity multi-disciplinary design optimization were used to size all aircraft. Results demonstrated a 13-30% increase in the flight range depending on the aircraft concept. Long-range jets with NLF could not achieve significant range extension due to a combination of the design airspeed and maintenance costs. A rapid increase in acquisition prices for all aircraft suggested that super mid-size and large jets that combine relatively low empty weight and high range extension could be more favorable options compared to other segments, but a significant reduction of acquisition costs and an increase in operating flight hours are required to make the technology implementation successful.

I. Introduction

The business jet market is a relatively small but highly competitive arena. Every manufacturer is continuously working on aircraft performance and systems improvements to offer maximum customer comfort with the best flying capabilities. Present improvements in modern business jets are mostly related to improvements in systems for passenger comfort and safety, avionics, and flight control systems. Similar to commercial aircraft, modern business jets are approaching their performance limits since existing technologies and the aircraft configuration which features them have been developed for a significant amount of time. More advanced airframe technologies are not only challenging from the development standpoint but also introduce significant risks to a manufacturer in terms of potential returns of investments into an aircraft with one or several unconventional technologies.

*Graduate Research Assistant, Institute of Aircraft Design and Lightweight Structures, s.karpuk@tu-braunschweig.de.
†Professor, Department of Aeronautics and Astronautics, Computational Engineering and Design Group, a.elham@soton.ac.uk

From the perspective of a commercial jetliner, minimum possible operating costs with maximum possible performance are of major interest for airlines and are a major goal of aircraft manufacturers. In addition, current research and development have also started focusing on technologies dedicated to more environmentally-friendly aircraft ranging from regional aircraft to long-range commercial jets. For business aviation, operating costs are also important, but aircraft performance becomes a more valuable characteristic since business aviation is dedicated to customers that can afford to spend extra money for their transportation convenience. Consequently, new technologies for business aircraft may have success in the business aviation market if they provide significant performance or passenger experience improvement and are not extremely expensive for the manufacturer to mitigate risks related to the program's success. In addition, new airframe or propulsion technologies that are commercially interesting for large passenger jets may not necessarily be viable for the business aviation market.

Aircraft and engine manufacturers are continuously improving technologies to maximize aircraft fuel efficiency. From the airframe perspective, reduction in zero-lift drag (C_{D_0}) is one of the major contributors toward a more fuel-efficient aircraft that can reduce Direct Operating Costs (DOC) due to less required fuel if the drag reduction technology is not excessively expensive to maintain. From the business-jet market perspective, a reduction in drag may enable the aircraft to extend its range without an increase in DOC due to the aircraft's overall higher efficiency.

Extension of the laminar flow around the aircraft can significantly reduce the C_{D_0} and increase the aircraft's fuel efficiency. The aircraft laminar boundary layer can be extended in two ways: aerodynamic shaping of the lifting surface to delay the adverse pressure gradient as much as possible to achieve a natural laminar flow (NLF) or to utilize active flow control (AFC) where the boundary layer suction is applied to delay the transition. Two approaches can also be combined to have a hybrid laminar flow control (HLFC) approach. Investigations of HLFC is being currently under active investigation and multiple recent research articles address the theoretical [1–4] and experimental[5] analyses, design [6–9], and operations [10] of HLFC airfoils and wings. Both AFC and NLF methods have their benefits and drawbacks. While the AFC can virtually keep the flow laminar as long as required if sufficient energy is applied, the system integration and structural design of the airframe with such systems are excessively complex and is currently limited to research airplanes for flight-test experiments [11]. The NLF relies only on the aerodynamic shaping of the airframe and its smoothness. However, achieving a smooth surface quality for a production-level aircraft is generally not an easy task, given that roughness created by the deicing/anti-icing system and skin waviness that can prematurely transition the flow [12]. Moreover, in the case of transonic flight where a moderate wing sweep is required, cross-flow instabilities add additional complications to already existing Tollmien-Schlichting instabilities. Mutual interactions of those two phenomena can be a challenging design task to maximize the wing laminar flow [3].

On the other hand, continuous advances in NLF have substantially increased the knowledge and understanding of the mechanism of NLF applied to aircraft analysis and design. Multiple high-speed aircraft configurations with significant assessments of NLF have been proposed by various researchers [13, 14], and methods that help integrate the technology

[15, 16] have recently been proposed. Operating uncertainties regarding the instability of the NLF during the flight [17] and effects of contamination on the flight mission [18] were also assessed to strengthen the understanding of NLF technology implementation for large aircraft. Advances in the design of composite structures showed the potential to successfully apply NLF for configurations that were not commonly used before. Studies performed by DLR showed that aeroelastic tailoring might enable NLF for a more aerodynamically favorable forward-swept configuration without weight losses due to the static divergence phenomenon [19, 20]. Finally, surface manufacturing applicable for NLF has shown that careful surface treatment may enable NLF for a rather large aircraft, which makes the application of NLF wider. One of the recent structural configurations proposed by DLR under the Clean Sky 2 NACOR project features a smooth transition between the nose and the wingbox skin [21]. The demonstrator was manufactured, and the skin structure has also been tested for waviness [22]. Two components are connected internally, and the gap is carefully filleted with a composite wedge. These outcomes show that despite complexities in the design and manufacturing of NLF wings for high-speed aircraft, there is a potential to introduce these technologies into more market segments. On the other hand, the production and maintenance of such technologies will definitely be complicated for large jets. Additional issues include surface quality maintenance combined with a busy fleet schedule.

Unlike large jets, a typical business jet aircraft has a substantially smaller wing planform which can make the implementation of the technology easier. Moreover, the business aircraft operating schedule is not as aggressive as commercial jets, so maintenance and surface cleaning requirements will be easier. Therefore, that gives the potential for this technology to be implemented into the business jet market technologically easier than for commercial jets if the performance and cost benefits can be achieved. However, the present research has assessed the possibilities of NLF application to business jets in a very limited fashion. Nangia [23] only briefly mentions potential applications of NLF for forward-swept aircraft of various types, including executive jets. Quagliarella [24, 25] and Strurdza [26] discuss aerodynamic design of supersonic business jets with NFL technologies. Somers [27] demonstrated the aerodynamic design of an NLF slotted airfoil for business jet applications. Finally, Fujino [28] discusses the NLF program performed for the design of the HondaJet lightweight business jet. The information about the potential of NLF technology implementation for a wide range of business-jet market segments is not currently available, which creates several questions:

1) Which aspects of airplane improvements that can be achieved by the implementation of NLF may have the highest interest to a potential customer?
2) How may the introduction of NLF technologies change the aircraft price, and can the price be competitive compared to existing aircraft?
3) From currently studied and developed configurations, what potential aircraft configuration can benefit the most from the NLF introduction?

The present research focuses on the investigation of the potential benefits of the NLF for aircraft in the business jet

market and tries to answer the questions stated above. The work is divided into several sections. Section 2 describes the evaluation metric that is going to be used for the present study to answer given questions. Section 3 investigates what parameters related to evaluation metrics are more interesting to the customer from the perspective of the aircraft price and if the range extension is a favorable strategy to focus the business jet aircraft design on. Section 4 summarizes top-level aircraft requirements (TLARs) for a selected range of business jets: from light to ultra long-range jets. Section 5 describes the design methodology and important assumptions. Section 6 describes configurations considered for each business jet category, and Section 7 discusses obtained results.

II. Aircraft evaluation criteria

Before answering the questions of the present research, a universal set of evaluation metrics need to be introduced. A widely used metric for the business jet performance evaluation is the Productivity Index (PI), defined by

$$PI = \frac{R_{LRC} M_{LRC} V_{cab}}{TOFL} \tag{1}$$

where R_{LRC} is the range at the long-range cruise speed (payload of 4 passengers (PAX) for very light to large categories and six passengers for ultra long-range jets), M_{LRC} is the long-range cruise Mach number, V_{cab} is the cabin volume excluding the cockpit and the baggage volume, and $TOFL$ is the take-off field length. Combined with the aircraft price, the relation between the two values can be generated and used as a metric for the aircraft value (where higher PI with lower price is a more valuable aircraft) and comparison among several aircraft.

From the airframe perspective, reduction in zero-lift drag (C_{D_0}) is one of the major contributors toward a more fuel-efficient aircraft that can reduce Direct Operating Costs (DOC) due to less required fuel if the drag reduction technology is not excessively expensive to maintain. From the business-jet market perspective, reduction in drag may improve the aircraft productivity in multiple ways: the aircraft range can be extended without an increase in DOC, the aircraft can cover the mission at a slightly higher cruise Mach number without extra fuel burn, or the business jet cabin can be enlarged to maximize customer experience without affecting the performance and DOC of the aircraft. Therefore, it is important to investigate which parameter of the PI index has more interest to a potential customer, so the NLF technology can be assessed for the goal, which is likely to be interesting for the market.

III. Determination of aircraft price drivers and the design objective

To investigate if the NFL plays an important role in the business jet market, it is first important to know what parameters influence the price the most and what the aircraft price sensitivity to these parameters is. To quantify the customer interest, it can be assumed that the aircraft acquisition price variation is a measure of customer interest for a given aircraft performance or geometric characteristic if the price of the aircraft remains inside the range of existing

aircraft prices. For instance, if the sensitivity of the aircraft price is significantly influenced by the aircraft's maximum range, which in turn can be improved by the introduction of the NLF wing, then the NLF option may have a benefit in the business jet market. On the other hand, if the parameter does not show a significant increase in the aircraft price or other weakly sensitive to the NLF characteristics show substantially more benefit than parameters proportional to the NLF, then the application of the technology will not have potential market benefits. However, it is important to ensure that the price sensitivity remains within the range of applicable prices provided by existing aircraft, which indicates that the customer is likely to purchase this aircraft.

To determine the aircraft price variation with aircraft characteristics, a model which enables such comparison must be introduced. Various models can be defined based on the importance of certain geometric and performance parameters. The definition used by Isikveren [29] was used in the present research, which defines the aircraft acquisition price as

$$Price = f(R_{LRC}, M_{MO}, V_{cab}, S_{cab}, TOFL) \tag{2}$$

where f is an arbitrary function created based on existing aircraft in the market. Here, f depends on the flight range at the long-range cruise speed R_{LRC}, the maximum operating Mach number M_{MO}, the cabin volume V_{cab}, the cabin slenderness S_{cab}, and on the take-off field length $TOFL$. V_{cab} is the cabin volume defined by

$$V_{cab} = \frac{L_{cab}}{4}\left[W_{cab}(\pi H_{cab} + \theta_c W_{cab}) + H_s(2W_{fl} - \pi W_{cab})\right] \tag{3}$$

In Eq. 3, L_{cab} is the cabin length, W_{cab} is the cabin width, H_{cab} is the cabin height, W_{fl} is the cabin floor width, H_s is the residual vertical height from the maximum width line to the floor defined by

$$H_s = \frac{1}{2}\sqrt{W_{cab}^2 - W_{fl}^2} \tag{4}$$

and θ_c is the angle between the maximum width line and the cabin floor defined by

$$\theta_c = \arctan\frac{2H_s}{W_{fl}} \tag{5}$$

Having a sufficient number of airplanes and obtaining their geometric and performance characteristics, a surrogate model of Eq. 2 can be created, which then is used for the sensitivity analysis. To evaluate the price sensitivity to selected aircraft variables, its partial derivatives can be approximated using a finite difference approach evaluated at the price of a given reference aircraft against which the comparison of each aircraft design will be performed.

A set of currently in-service light, mid-size, super-midsize, large, long- and ultra long-range business jets characteristics and their approximate prices have been obtained from online resources, pilot operating manuals, and

brochures. For light jets, the database of airplanes includes Syberjet SJ30i, Embraer Phenom 300, Pilatus PC-24, Cessna Citation Jets 3+ and 4, Learjet 75, and Hawker 400 XP. Mid-size jets are represented by the Embraer Legacy 450 and 500, Embraer Praetor 500, Cessna Citation X, Sovereign, Latitude, and Longitude, and Gulfstream G100. Super mid-size jets include Bombardier Challenger 300 and 350, Gulfstream G250, Embraer Praetor 600, and Dassault Falcon 2000S. The large jet category includes Bombardier Challenger 650, Gulfstream G350 and 450, Embraer Legacy 600 and 650, and Dassault Falcon 900 LX. Finally, long- and ultra long-range jets include Gulfstream jets from G500 to G800, Dassault Falcon jets from 6X to 10X, and Bombardier jets from Global 5500 to Global 7500. A total database of 46 jets was created to build a surrogate model which determined parameters that affect the aircraft acquisition prices in each class. In addition, since the aircraft acquisition price also plays an important role in potential aircraft market applicability, proper price bounds for the future aircraft must be set to determine if the aircraft can be applicable to the given market. Figure 1 shows a chart with acquisition prices of selected aircraft versus the PI. Price estimates for selected jets were obtained from the online database Air.one [30]. Clouds on the chart represent a typical range of aircraft PI values and prices for each business jet market segment. Finally, two solid black lines represent price bounds for future aircraft. Both upper and lower bounds were selected based on the minimum and maximum prices for each category. The linear approximation of the price variation was used similar to Ref. [29]. If the future aircraft does not fit within the boundaries, then its market success most likely is impossible due to an excessive price difference compared to its competitors. From the maximum price standpoint, the aircraft will be too expensive, and its performance benefits may not be worth the money. It must also be noted that although the linear function was used for the upper price bound, the price shall also be compared against existing aircraft that may not be close to the upper price limit, as can be observed for the ultra long-range family. The minimum price is less strict and indicates an excessively low price for a given aircraft. If the minimum price limit for the new aircraft is reached, then it can be easily increased to increase the profit more.

To create a surrogate model based on the existing database, the Regression Learner Toolbox available in MATLAB was used. Out of available regression models, the Gaussian Process Regression algorithm showed the smallest root-mean-square error (RMSE) among other algorithms and was equal to 3.0. Figure 2 shows a comparison of predicted and actual price values for all selected aircraft. Overall, given a limited amount of aircraft in the database, obtained results show a satisfactory level of accuracy.

The most influential parameters on the aircraft can be obtained by a surrogate model of the acquisition price as a function of aircraft variables. To perform the given task, reference aircraft must be selected. For the light jet category, the Embraer Phenom 300 was selected as the best-selling aircraft in the category. For the mid-size jet, the Praetor 500 was chosen as the best performing airplane in the class, whose PI is equal to 87. For the super mid-size jet, the Praetor 600 was selected. Although Dassault Falcon 2000S has a slightly larger PI value, Praetor 600 features a significantly longer range and does not have a substantially smaller cabin volume compared to the assault Falcon jet. This combination of

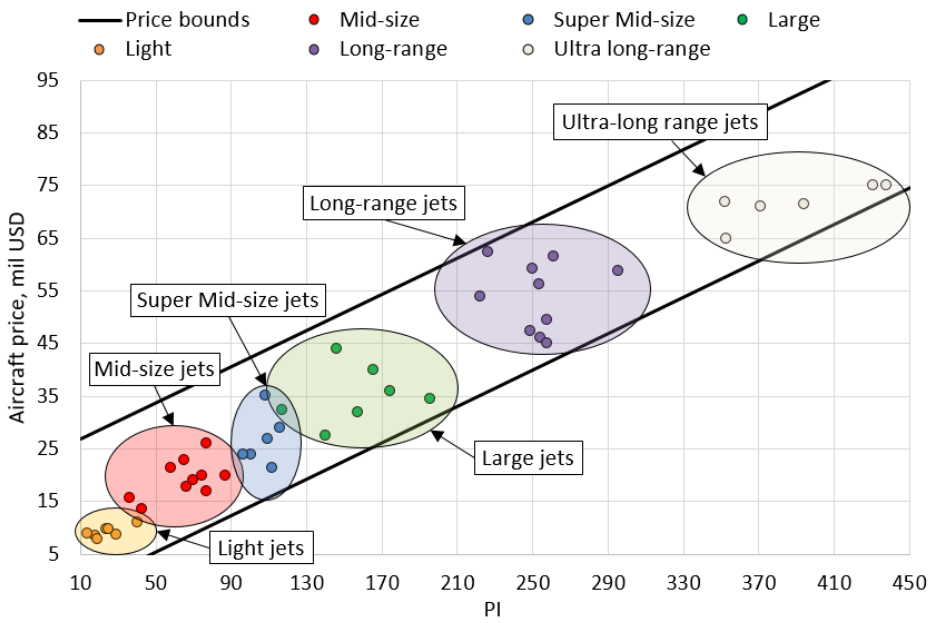

Fig. 1 Productivity Indices versus acquisition prices for selected segments of the business jet market.

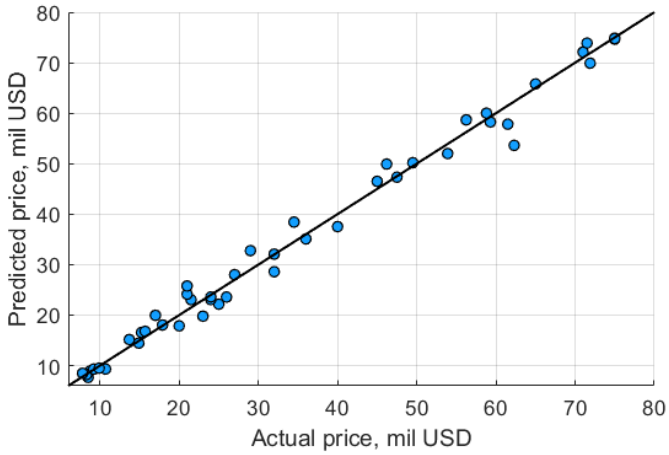

Fig. 2 Comparison of acquisition prices for selected aircraft using the Gaussian Process Regression algorithm.

aircraft characteristics gives the Praetor 600 the value of 114.4, which brings it to second place among super-midsize aircraft and is almost similar to the Dassault Falcon 2000S. For the large jet, the Embraer Legacy 650 was selected. Although its PI is the third in the class after Gulfstream G350 and almost similar to G450, its price is substantially lower than G450, and it also features a longer fuselage which is easier to use for investigation of different wing configurations, as it will be discussed later. G600 was selected for long-range jets because it has one of the longest ranges among airplanes in the class, features a relatively moderate price, and has the one with the highest PI indices. Finally, G800 was used for the ultra long-range segment as the aircraft with the longest range in the class and moderate productivity index.

The goal of the sensitivity analysis is related to an investigation of the average market price trends depending on

the aircraft's geometric and performance characteristics. However, partial derivatives may significantly depend on the point within the surrogate model, so the overall market image is not well-observed. To observe a general market trend, average partial derivatives for each market segment from light to large jets were taken. The average partial derivative is defined by

$$\overline{\frac{\partial Price}{\partial x}} = \frac{\sum_{i=1}^{N} \frac{\partial Price_i}{\partial x}}{\sum_{i=1}^{N} i} \tag{6}$$

where x is the aircraft characteristic and N is the number of aircraft in the database. Assuming that the designed airplane must satisfy the TOFL requirement of a reference aircraft, all remaining variables were changed by 5% with respect to reference values. Figure 3 shows changes in acquisition prices of reference aircraft with respect to the aircraft range at the maximum range cruise speed, maximum Mach number, and fuselage geometric characteristics.

Results demonstrate different trends for each market segment. All market segments show that the long-range cruise distance R_{LRC} almost always plays the most important role in the price of an aircraft. For light jets, the range absolutely dominates the market compared to other price drivers. For mid-size and super mid-size jets, the maximum cruise Mach number M_{MO} plays a significantly more important role compared to other parameters, but the range was still the most influential one. For large jets, M_{MO} showed more effect on the price compared to the range, while the range had the second most important influence. Finally, long- and ultra long-range jets showed the range as the most dominant price driver, with the M_{MO} being the second driver.

From the two most important design parameters (R_{LRC} and M_{MO}), the aircraft range is directly affected by the NLF, while the maximum Mach number is driven more by the drag divergence Mach number which depends on the compressibility drag, so the benefit of NLF may not be as pronounced. Consequently, the range extension was selected as the design goal of NLF business jets. Moreover, the objective for sizing each business jet includes the maximization of the range at a similar DOC per year with respect to the reference aircraft, so a more operating cost-effective aircraft are obtained. For each market segment, several configurations will be considered to investigate their cruise range extension potentials, ranges of PI, and aircraft price applicability. The outcome will conclude how much NLF design concepts can extend their range with respect to reference aircraft, how much their productivity is increased, if NLF can be price-feasible for given price constraints, and what configurations among currently existing or previously designed ones will have the best price-productivity combinations for each market segment.

IV. Aircraft top-level requirements and configurations to consider

Top-level aircraft requirements (TLARs) for five business jets are summarized in Table 1 and are based on selected reference aircraft used for the price sensitivity analysis: Embraer Phenom 300, Praetor 500, Praetor 600, Legacy 650, and G600. As mentioned earlier, the design will focus on maximizing the aircraft range without changes in DOC. Cabin

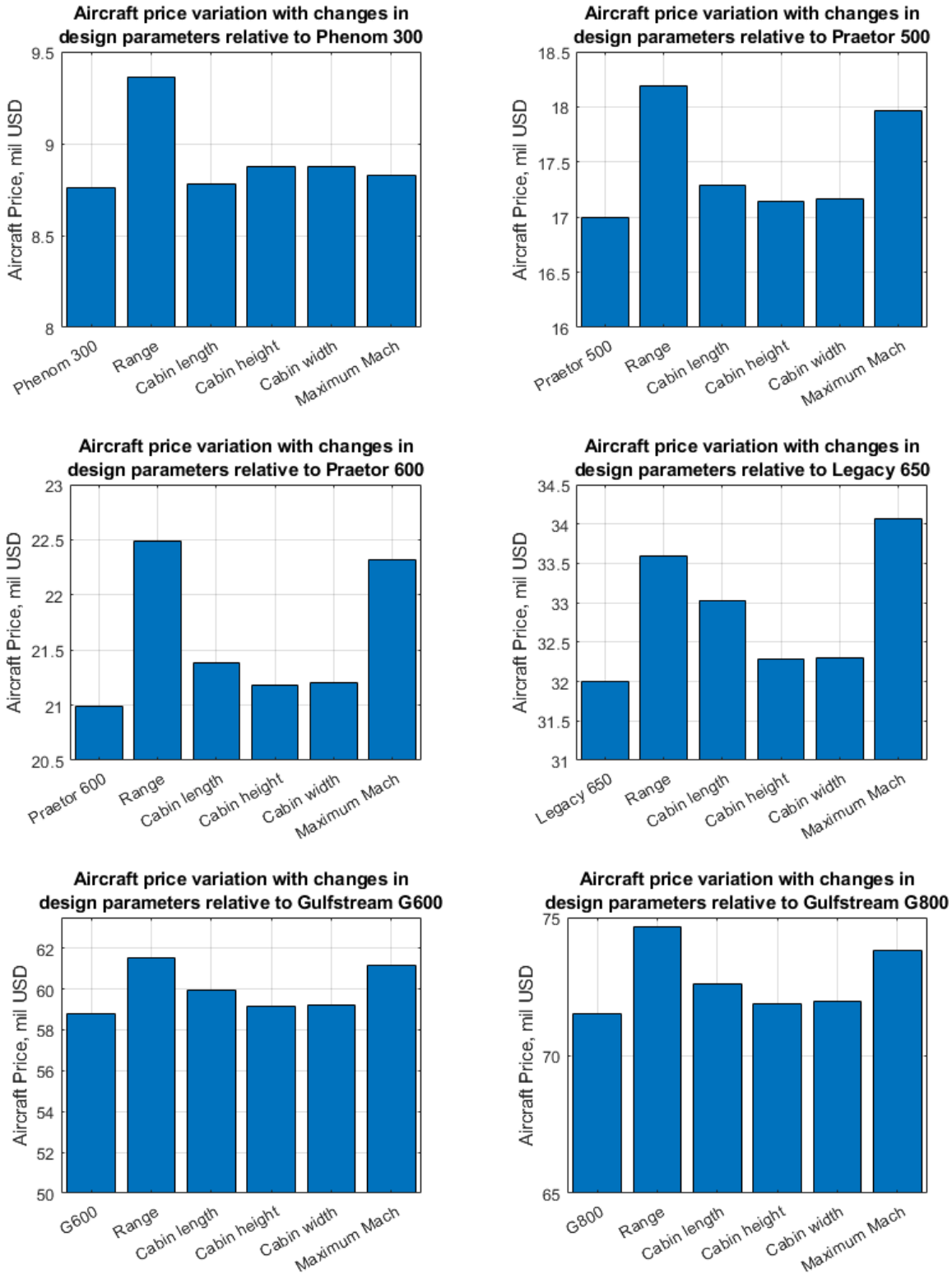

Fig. 3 Aircraft price sensitivity of four reference aircraft with respect to design characteristics.

dimensions will remain constant for all aircraft to offer similar cabin characteristics to reference aircraft. The mission profile includes the main mission, a 200 nmi reserve, and a 30 min hold at 450 m [31].

Table 1 Top-level requirements for business jets of four different categories.

Parameter	Light	Mid-size	Super Mid-size	Large	Long-range	Units
Maximum PAX	6	9	12	14	19	-
M_{LRC}	0.76	0.78	0.78	0.78	0.85	-
M_{MO}	0.80	0.83	0.83	0.80	0.90	-
Service ceiling	13716	13716	13716	12500	15545	m
Take-off field length	978	1287	1352	1750	1737	m
Landing distance	674	636	692	866	945	m
Certification			CS-25 [32]			

Table 2 Aircraft configurations considered for the initial business jet sizing

Light	Mid-size / Super mid-size	Large / Long-range
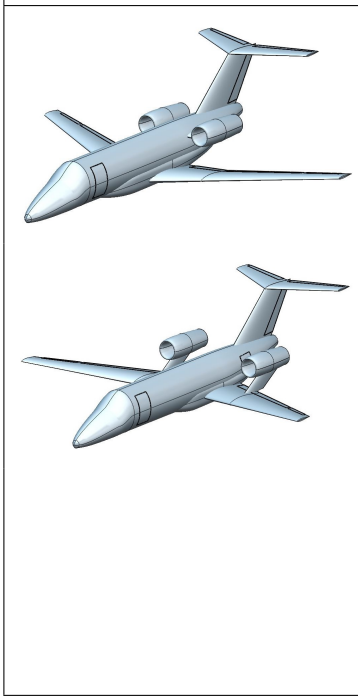	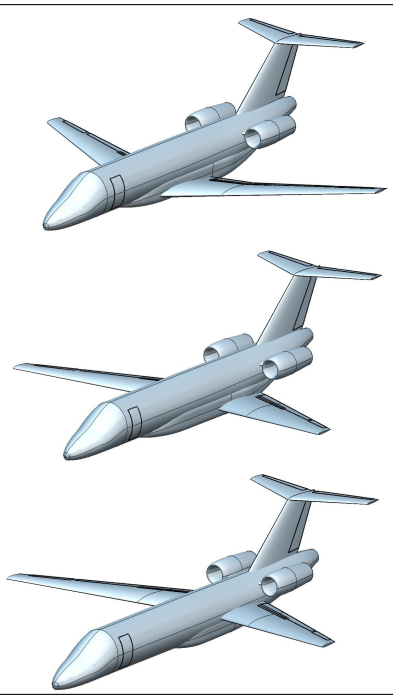	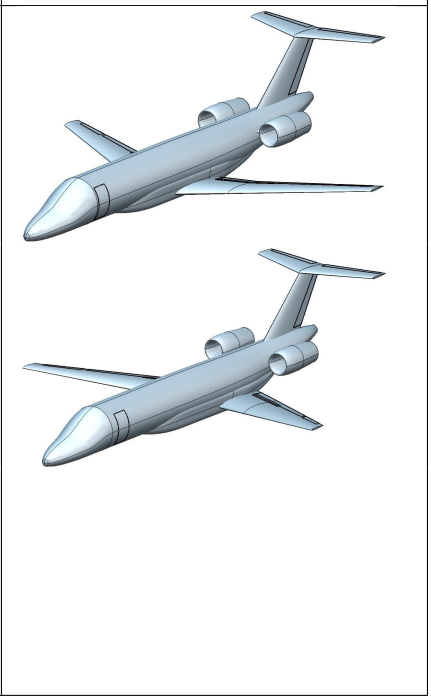

Several configurations have been selected for the initial sizing to observe the potential influences of different configurations with NLF wings on the market accessibility. Table 2 presents potential configurations for each category. For the light jet, the classical backward-swept wing with fuselage-mounted engines and forward-swept wing with wing-mounted top engines similar to the HondaJet [28] were selected. For the wing-mounted engine configuration, it is assumed that the aft fuselage space, where fuselage-mounted engines are generally located, is used for the baggage compartment, while the wing is located slightly higher than the conventional low wing, and the main spar is located

aft of the pressure bulkhead. This way, the belly fairing size can be minimized to reduce fuselage drag. For both mid-size and super mid-size jets, three configurations are considered: the conventional backward-swept wing with fuselage-mounted engines, a low-mounted forward-swept wing with fuselage-mounted engines, and the configurations similar to the second one, but with the mid-wing arrangement to reduce the fuselage maximum cross-sectional area. For the last configuration, a substantially smaller belly fairing is devoted for a small fuel tank and the landing gear, while most of the fuel is located in the wing and the mid section aft of the pressure bulkhead. The configuration, however, will have a smaller baggage compartment which will be measured and considered during the trade study. Finally, for the large and long-range jets, locating the wing aft of the pressure bulkhead is substantially more difficult due to a long cabin. Consequently, two configurations with low-mounted backward- and forward-swept wings are considered.

V. Design methodology and assumptions

A. Initial aircraft sizing

The conceptual design was performed using various tools. OpenVSP [33] was used for the aircraft geometric modeling, allocation of critical systems, and their mutual arrangements. SUAVE [34] was used for the aircraft sizing, performance, and mission analysis. The initial sizing within SUAVE features constraint diagram developed as initialization using methods described by Gudmundsson [35], the mission simulation, and classical performance analysis routines described in Ref [35–38]. Features of the constraint analysis and performance scripts were developed internally as an extension of basic SUAVE mission analysis and aircraft sizing capabilities.

The initial aircraft sizing within SUAVE is performed iteratively, as shown in Figure 4. First, geometric specifications such as the wing aspect and taper ratios, sweep, airfoils, high-lift devices, propulsion system, tail volume ratios, and initial guessed weights are initialized. In addition, a set of TLARs and a sample mission profile are initialized. Next, SUAVE performs the constraint analysis to select the first combination of thrust-to-weight ratio (T/W) and wing loading (W/S). Two design point selection criteria are possible: for the minimum T/W and for the maximum W/S. Selected wing loading and thrust-to-weight ratio are used to run the SUAVE mission analyses to estimate the aircraft's performance and its required fuel weight which is then used to estimate the aircraft's maximum take-off mass (MTOM). Obtained weights and propulsion system characteristics are used to calculate DOC using the method presented in Ref [39]. Obtained total DOC for a user-defined number of flight hours per year is compared against the reference aircraft DOC obtained using SUAVE. Similarly, MTOM is compared against the value at the previous iteration and is updated if the tolerance is not reached. After the tolerance check, a relative change in yearly DOC per cruise distance is calculated to calculate the new cruise flight range to match the reference DOC. Finally, the next iteration is performed using updated aircraft geometric and propulsion characteristics. Parameters such as the minimum drag coefficient (C_{Dmin}), Oswald efficiency (e), and maximum lift coefficient ($C_{L_{max}}$) for clean and flapped configurations are input into the

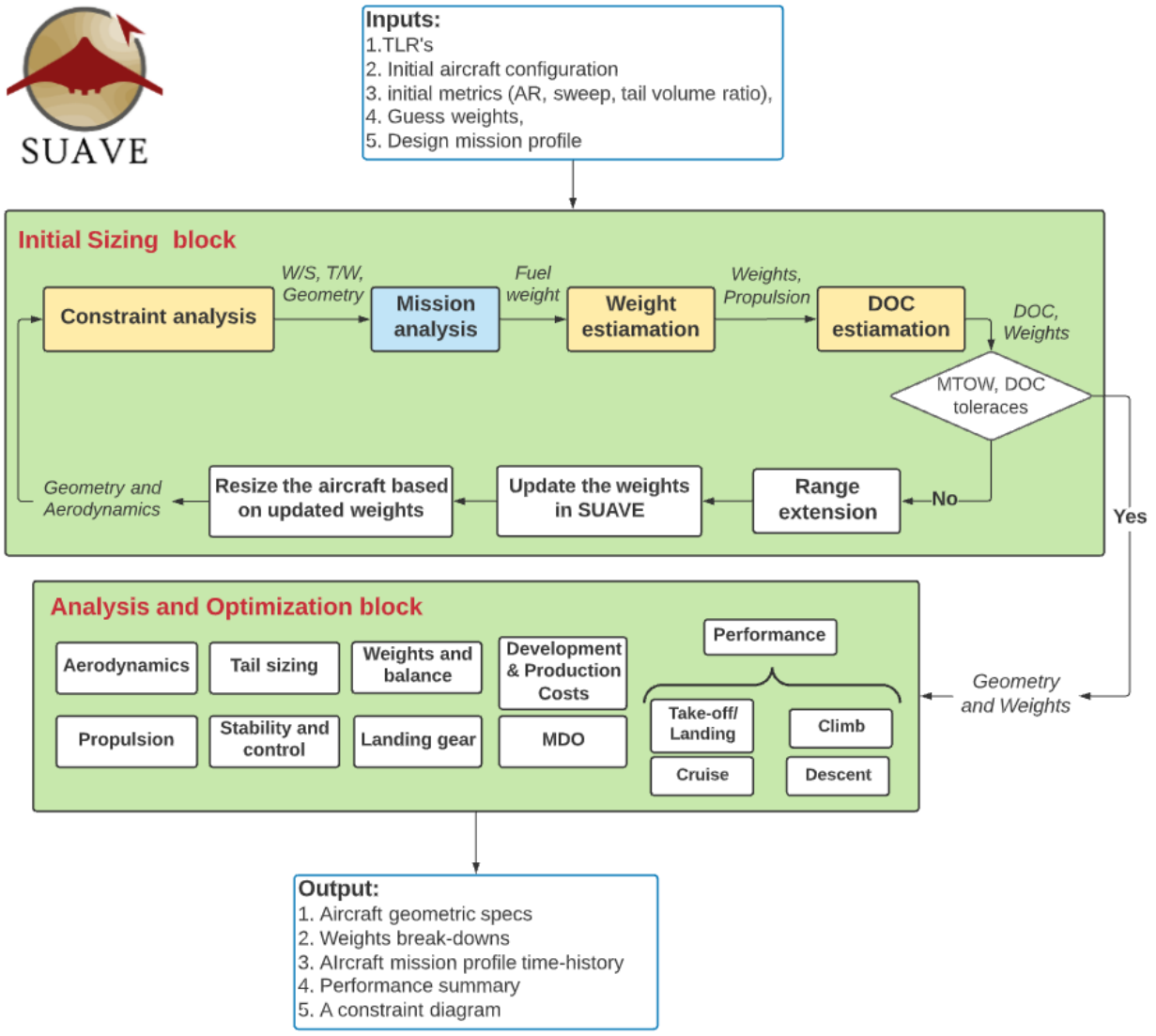

Fig. 4 Initial aircraft sizing framework using SUAVE

constraint diagram again to update all constraint curves and runs the next iteration. The solution is terminated when the change in the aircraft MTOM and the difference between the designed and the reference aircraft DOC are reached.

After the initial sizing using the constraint analysis is finished, the program moves to the aircraft refinements block to update the existing configuration and include analyses that were not covered by the initial sizing block. Refinements include more detailed aerodynamic analysis, performance assessments, tail sizing, sizing of landing gear, etc. Methods of Torenbeek [37] and Roskam [38] are used within SUAVE to analyze various types of leading- and trailing-edge devices. The empennage sizing within SUAVE is based on the fixed tail volume ratio based on existing reference aircraft. Performance analysis scripts within SUAVE included take-off, all engines operative (AEO), and one engine inoperative (OEI) climb, cruise, descent, and landing.

Finally, an additional refinement using a low-fidelity multi-disciplinary design optimization (MDO) is performed.

The objective of the present problem is to maximize the flight range with similar to reference aircraft DOC by varying the wing geometry and the engine thrust-to-weight ratio. Constraints for the optimization problem correspond to aircraft performance characteristics defined in the TLRs, performance requirements prescribed by the constraint analysis, a wingtip geometric constraint to ensure manufacturability of the wing, and the wing minimum allowable fuel volume to ensure sufficient overall fuel volume and adequate fuel distribution which will ensure satisfactory aircraft balancing. Tables 3 and 4 describe the formulation of the optimization problem. There, C_r and C_t are the wing root and tip chords, respectively, t/c is the wing thickness, Λ_{LE} is the wing leading edge sweep, V_{fuel} is the fuel volume within the wing, $V_{fuel,ref}$ is the wing fuel volume of the reference aircraft, b is the wingspan, and $\eta_{maxcruise}$ is the maximum throttle during the flight at the maximum cruise speed. The maximum throttle is used as an indicator of sufficient engine sizing to meet the requirement of the maximum cruise speed flight.

Table 3 Optimization problem definition for mid-size, super mid-size, and large business jets. Values in parentheses indicate bounds for backward-swept wing configurations.

		Lower	Upper	Units
maximize	R_{LRC}			
wrt	AR	7.00	11.00	
	λ	0.25	0.45	
	C_r	2.00	4.00	m
	$t/c\|_{root}$	0.11	0.14	
	$t/c\|_{tip}$	0.09	0.12	
	T/W	2.5	4.5	N/kg
	Λ_{LE}	-20.0 (15.0)	-15.0 (30.0)	deg
subject to	Take-off field length (TOFL)		TLR TOFL	m
	Landing field length (LFL)		TLR LFL	m
	$\eta_{maxcruise}$		1.0	
	C_t		1.0	m
	V_{fuel}		$V_{fuel,ref}$	m^3
	b		b_{ref}	m
	$DOC - DOC_{ref}$	0.0	0.0	USD/year

For the MDO, the leading edge sweep angle and taper ratio were limited using several initial considerations. For backward-swept wings, to avoid excessive tip loading, both wing taper and wing sweep were limited to 0.25 and 30° respectively for lower-speed aircraft, while high-speed aircraft had a wing sweep limit of 40°. For forward-swept wings, the taper ratio as a contributor to the tip loading is not as critical as for backward-swept wings due to the root-dominant lift distribution. However, forward-swept wings have a lateral destabilization effect on the aircraft. According to Scholz, 10° positive sweep achieves approximately as much as 1° dihedral. Moreover, typical wing dihedral angles for unswept wings range between 5° and 7° and between 2° and 4° for the low wing and mid wings, respectively [40]. Sweeping the wing forward means that the wing needs to increase its dihedral to roughly compensate for the destabilizing effect.

Table 4 Optimization problem definition for long- and long-range business jets. Values in parentheses indicate bounds for backward-swept wing configurations.

		Lower	Upper	Units
maximize	R_{LRC}			
wrt	AR	7.00	11.00	
	λ	0.25	0.45	
	C_r	4.00	8.00	m
	$t/c\|_{root}$	0.11	0.14	
	$t/c\|_{tip}$	0.09	0.12	
	T/W	2.5	4.5	N/kg
	Λ_{LE}	-25.0 (25.0)	-15.0 (40.0)	deg
subject to	Take-off field length (TOFL)		TLR TOFL	m
	Landing field length (LFL)		TLR LFL	m
	$\eta_{maxcruise}$		1.0	
	C_t		1.0	m
	V_{fuel}		$V_{fuel,ref}$	m^3
	b		b_{ref}	m
	$DOC - DOC_{ref}$	0.0	0.0	USD/year

Using these relations and limiting maximum dihedral to 8°-9° for a low wing to avoid excessive dihedral angles that may significantly increase yaw-roll coupling, the maximum forward sweeps angle of $-20°$ was obtained for lower speed aircraft and $-25°$ for high-speed airplanes to ensure sufficient sweep to minimize compressibility drag. It is important to note that such assumptions are rather conservative to avoid overly optimistic results of initial designs. However, depending on the final design outcomes, a more detailed stability and control analysis must be performed. The fuel volume constraint was based on the available volume of reference aircraft and was estimated using SUAVE. Finally, the wingspan constraint b was made relatively relaxed to investigate the potential increase in the aircraft wingspan due to the effect of laminarization. Constraints for each market segment were based on the Annex 14 regulation [41]. Table 5 summarizes wing fuel volume and wingspan constraints for each market segment.

Table 5 Reference aircraft wing fuel tanks volumes and wingspan constraints.

Parameter	Light	Mid-size	Super mid-size	Large	Long-range	Units
$V_{fuel,ref}$	2.4	4.1	5.0	6.3	23.5	m^3
b_{ref}	24.0	24.0	24.0	24.0	36.0	m

To perform the MDO, SUAVE was coupled with MATLAB, and the Genetic algorithm was used to find optimal solutions. To account for the constraints, the penalty function similar to one defined in Ref [42] was used. The penalty function is defined by

$$f_p = \mu(y - y_c)\left(\frac{y}{y_c}\right)^3 \tag{7}$$

where y is the design variable, y_c is the design variable constraint, and μ is the unit step function equal to zero for $y \leq y_c$. With the introduction of the penalty function, the objective function becomes

$$f = f + \sum_{i=1}^{N} f_p \tag{8}$$

where N is the total number of design variables. Seventy species per generation were set to have a sufficient population size without major accuracy losses. Take-off and landing constraints were calculated using physics-based time-dependent performance formulations described by Gudmundsson [35].

B. Calibration of FLOPS weight estimation for business jets

To estimate aircraft weights, the FLOPS [43] method was used within SUAVE. One of the major concerns related to weight estimation at the conceptual design stage is related to uncertainties of the model for a given type of airplane. For instance, business jet furnishing and cabin systems may not be well-represented by the FLOPS weight estimation method. Consequently, since aircraft weights play an important role in the estimation of the new aircraft range benefits, an empty weight calibration was performed.

The FLOPS model empty weight estimation was calibrated with respect to several aircraft in the database. Twenty-seven airplanes were used for the empty weight calibration. Aircraft weights and engine characteristics were obtained from corresponding operating manuals, brochures, and open official website information of each manufacturer while missing geometric parameters that were not explicitly described in official resources were measured using three-view aircraft drawings. It must be noted that not all parameters were possible to obtain even using drawings. For instance, the information about airfoils and the wing thickness distribution along the wing was not found. Therefore, a reference combination of thicknesses of 0.13 at the root and 0.1 at the tip were used for all aircraft, similar to thickness distributions described by Obert [44]. Finally, since the engine model in SUAVE is the physics-based method from Cantwell [45] and requires parameters for each major engine component, the default engine model in SUAVE was corrected based on the overall pressure ratio of each of business jet engines and its geometric characteristics to ensure that a similar final fuel burn rate is reached. All digitized airplanes were simulated in SUAVE to ensure that FLOPS obtained similar weights to the data available for given airplanes. To match the aircraft weights to their references, an empty weight gain ΔW_e was introduced. The weight gain accounts for differences in empty weights between the SUAVE output and actual aircraft empty weight, so the deviation of the original FLOPS is minimized. The corrected empty weight formulation is defined by

$$W_{e,SUAVE} = W_{e,FLOPS} + \Delta W_e \tag{9}$$

Knowing the distribution of the empty weight gain for each aircraft in the database, the weight gain distribution as a function of the empty weight can be obtained. Figure 5 shows ratios of the empty weight gain to the operating empty

weight $\Delta W_e/W_e$ for aircraft included in the database as a function of W_e. In the first figure, rounded rectangles represent each market segment, red lines show the bounds of the data cloud, and the blue line shows the least squares fit of the obtained data. the second figure represents the percent difference between the upper and lower bounds of the data cloud on the left. As shown in the figure, the weight gain distribution for each database aircraft has an uneven behavior. The empty weight gain ratio uncertainty between 5% and 8.5% exists depending on the aircraft empty weight. Such difference in the data creates uncertainty for the final range extension of aircraft to be designed, since the aircraft DOC depends on aircraft weights and the design problem is to extend the aircraft range to match the DOC. Consequently, the design sensitivity of the empty weight gain must be investigated during the initial sizing, so it becomes evident how much the error margin can be and if the least squares fit can be used as a universal solution for the present study. If the error margin does not show significant uncertainties, then the curve fit can be implemented into SUAVE as the initial sizing formulation.

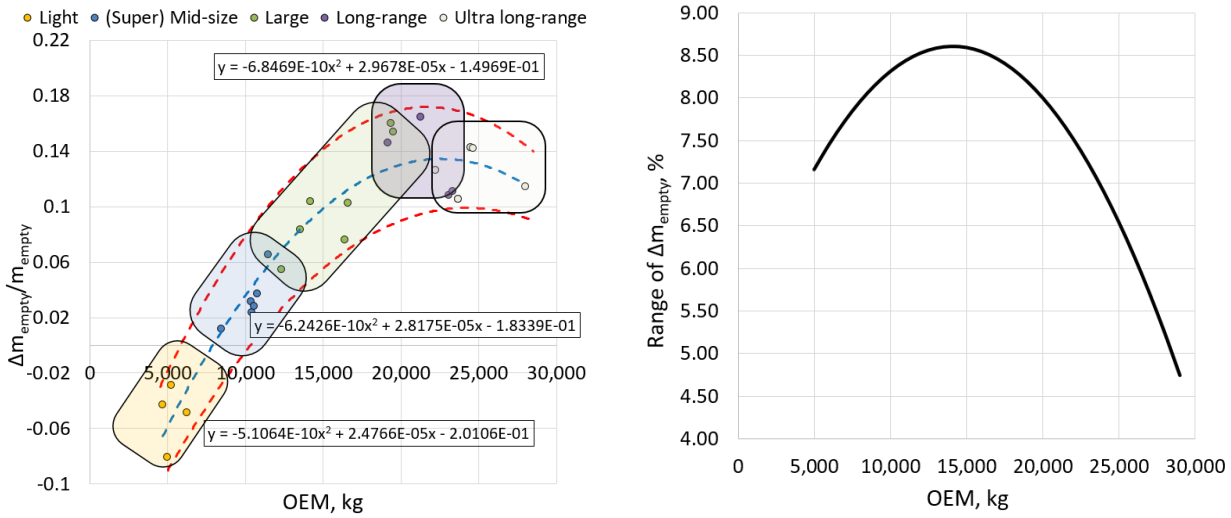

(a) Empty weight calibration change ratio. Blue line represents the least squares fit and red lines show the design data domain bounds

(b) Range of the empty weight calibration change ratio

Fig. 5 Change in the empty weight calibration as function of the aircraft empty weight.

C. Costs estimation

The estimation of aircraft costs is divided into two components. The first type of costs considered in the analysis which determines the aircraft range extension is the Direct Operating Costs (DOC). The method described by Hoelzen [39] was used to assess the DOC, which is defined by

$$DOC_{Total} = DOC_{Energy} + DOC_{Crew} + DOC_{Ma} + DOC_{Cap} + DOC_{Fees} \tag{10}$$

where DOC_{Energy} are costs of energy, DOC_{Crew} are crew costs, DOC_{Ma} are maintenance costs, DOC_{Cap} are capital

costs, and DOC_{Fees} are costs of fees. All costs were calculated in 2022 USD. Since the sizes of business jets are small and a rather narrow portion of 10-15% of the chord is required for cleaning and the process is generally not as complex as for large jets [46], the cost penalty due to the cleaning time was neglected.

Given methods for DOC estimation are based on conventional metallic aircraft. However, the maintenance cost of composite aircraft parts may vary from metallic parts significantly. Therefore, modifications to maintenance costs are required to account for aircraft composite materials maintenance. The maintenance part of DOC is defined by

$$DOC_{Ma} = (DOC_{AF,mat} + DOC_{AF,per} + DOC_{Eng})FC \tag{11}$$

where $DOC_{AF,mat}$ are material costs, $DOC_{AF,per}$ are labor costs, DOC_{Eng} are engine costs, and FC is the number of flight cycles per year. For the present research, due to the lack of detailed information and rapid methods to compare maintenance labor on metallic and composite parts, the labor costs are assumed independent of the material used. The material part of maintenance costs is defined by

$$DOC_{AF,mat} = m_{AF}(0.0010136t_{total} + 0.0012632) + k_{Rep} \tag{12}$$

where t_{total} is the flight time in hours, and k_{Rep} is the repair cost per flight. The airframe mass m_{AF} is defined by

$$m_{AF} = m_{OEW} - m_{Prop} \tag{13}$$

where m_{OEW} is the aircraft operating empty mass and m_{Prop} is the propulsion system mass. To account for price differences between metallic and composite materials, a correction factor to material costs must be introduced. As shown in Eq 13, DOC of material is directly proportional to the airframe weight. The airframe weight can be split into components such as the wing, the fuselage, the empennage, and aircraft systems. Each component can have a gain factor that corresponds to the DOC increase due to the use of more expensive materials, so the new material DOC becomes

$$DOC_{AF,mat,new} = DOC_{AF,mat} \sum_{i=1}^{M} \left(\frac{C_i m_i}{m_{AF}} \right) \tag{14}$$

where C_i is the material cost gain equivalent to the ratio between the new material price to the price of the reference material, m_i is the mass of each major aircraft component, and M is the number of airframe components. From Eq. 14, changes in material DOC is directly proportional to the weight of each airframe component and the material cost gain. Knowing what components are designed using specific materials, one can estimate a potential change in overall DOC. For all aircraft components except for the wing, conventional materials are used, so values of C_i are equal to one. For the wing, it is assumed that carbon fiber reinforced plastics (CFRP) are used, so complex shapes such as the upper skin

with the front spar can be manufactured and have high smoothness. The main concern is related to the value of C_i for such materials. The only reference presented by Dutton [47] suggests that the ratio between aluminum and CFRP row material costs is equal to 16.0, while finished material costs (for instance, manufactured parts such as ribs) have a ratio of 3.4 due to a large amount of waste during aluminum components machining. For maintenance, both raw materials for patches or local repairs and replacement of components may happen. Consequently, an average value equal to 10 was used for the cost gain due to the implementation of CFRP. Table 6 summarizes important DOC assumptions for the present work. It must be noted that presented metrics may be conservative, and a more detailed price costs comparison between metallic and CFRP materials shall be done in the future.

Table 6 DOC assumptions.

Parameter	Value	Reference
Fuel rate	5.00 USD/gal	[48]
Labor cost rate	70.8 USD/hr	[49]
CFRP cost gain	10.0	[47]
Crew rate	70800 USD/year	[49]
Pilot rate	177000 USD/year	[49]
Navigation fees	82.6 USD/year	[49]

To compare reference and designed aircraft, a fixed number of flight hours per year must be selected for both aircraft. A reference value of 450 hours per year was chosen for all benchmark and designed aircraft DOC estimations.

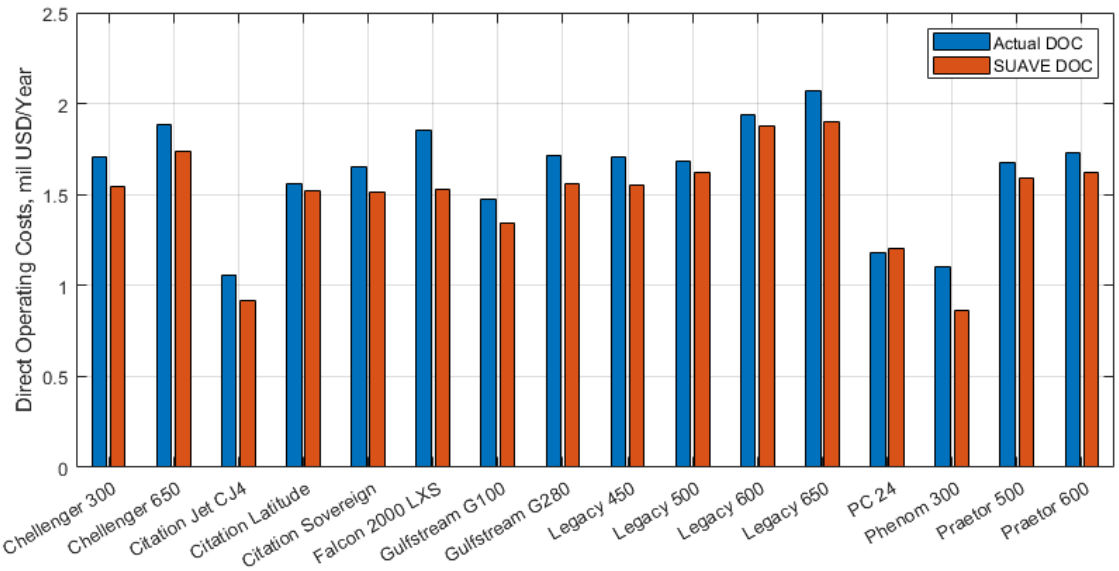

Fig. 6 Comparison between SUAVE-estimated aircraft DOC and DOC from the database for reference aircraft.

Validation of the DOC model was performed with respect to values estimated by the 'Compare Private Planes' online database [50], where the cost breakdown is estimated using an in-build cost estimation model. Figure 6 compares

results obtained using both methods for sixteen aircraft for 450 flight hours per year. Results demonstrate lower DOC for the SUAVE-embedded model compared to the reference resource for nearly all aircraft. Three aircraft demonstrate DOC differences of between 13% and 22% while other aircraft have errors not exceeding 10% with the majority having values of 5% and less. The average error for the complete set is equal to 5.3%. Due to complexities in DOC estimations and variations of models, differences are expected, but the general trend allows the model to be used for the analysis knowing that the majority of values do not exceed 10%.

The second type of cost used for the design assessment is the development and acquisition cost. The assessment of these costs determines if the aircraft price may be applicable to the market even though DOC benefits may be present. To ensure a potentially successful demand of the aircraft on the market, its development costs shall fit within the bounds of initially determined prices shown in Figure 1. Preferably, the aircraft price shall not significantly exceed the price of the reference aircraft to be more advantageous for the potential customer. Aircraft development costs were estimated using the method provided by Roskam[38]. Development and acquisition costs are divided into multiple components. Development costs are defined by

$$C_{RDTE} = C_{aed_r} + C_{dst_r} + C_{fta_r} + C_{fto_r} + C_{tsf_r} + C_{pro_r} + C_{fin_r} \tag{15}$$

where C_{aed_r} are airframe engineering and design costs, C_{dst_r} are development support and testing costs, C_{fta_r} are costs related to the manufacturing of flight test prototypes, C_{fto_r} are flight test operations costs, C_{tsf_r} are test and simulation facilities costs, C_{pro_r} is the profit embedded into the program, and C_{fin_r} are costs of financing. Acquisition costs are defined by

$$C_{ACQ} = C_{MAN} + C_{pro_m} = C_{aed_m} + C_{apc_m} + C_{fto_m} + +C_{fin_m} + C_{pro_m} \tag{16}$$

where manufacturing costs C_{MAN} are split into airframe engineering and design costs for manufacturing C_{aed_m}, airplane program production costs C_{apc_m}, production flight test operations costs C_{fto_m}, costs of financing during the manufacturing phase C_{fin_m}, and the embedded profit C_{pro_m}.

Multiple costs assumption has been made to design aircraft configurations. For all aircraft, the value C_{pro_m} was assumed 10% of final total costs, and C_{fin_m} also assumed 10% of total costs, similar to the recommendations of Roskam. To account for the effects of advanced technologies, the method of Roskam uses factors to estimate cost gains due to various material types and aircraft development complexity within the model. For moderately advanced technologies, Roskam recommends the factor of 1.5, while for aggressively advanced, the factor of 2.0 is recommended. Two aspects of NLF aircraft create design difficulties: manufacturing of the NLF structure and satisfaction of necessary tolerances and the integration of the technology into more unconventional aircraft. If the aircraft features a backward-swept

wing, most additional complexities are related to the design and manufacturing of the NLF composite wing, which is a moderately complex task compared to the design and manufacturing of conventional metallic wings. Therefore, the factor between 1.4 and 1.6 is used. The range of factors is used to capture sensitivities of costs to technology assumptions. If the wing is forward-swept and is mid-mounted, then the wing needs to be carefully tailored to avoid substantial weight penalties due to aeroelastic divergence mitigation. Moreover, the destabilizing nature of the forward-swept wing needs to be treated carefully by the airframe design and additional control system capabilities. Since the design complexity increases, it is assumed that factors between 1.5 and 1.7 are used. If the wing is forward-swept low-mounted wings, the destabilizing effects are stronger than for the mid-mounted ones, so all gains were assumed to be 0.05 larger than for mid-mounted wings. Finally, if over-the-wing mounted engines similar to HondaJet are used, an additional gain of 0.05 is assumed. Table 7 summarizes possible combinations of complexity assumptions. For the material gain factor, only the wing features composite materials. According to Roskam, the gain factor for composite materials for the complete aircraft range from 2.0 to 3.0. The amount of composite material used for the wing can be crudely approximated by the wetter area ratio between the wing and the complete aircraft. For business jets in the database, the ratio of wing wetter area to the total wetted area is approximately 0.33. Then, the material factor gain can be approximated as a linear function of the wetted area ratio

$$F_{mat} = k\left(\frac{S_{wet_{wing}}}{S_{wet_{total}}}\right) + m \tag{17}$$

where coefficients k and m are found using appropriate material cost gains boundary conditions. For the present study, the boundary conditions are

$$F_{mat} = \begin{cases} 1, & \left(\dfrac{S_{wet_{wing}}}{S_{wet_{total}}}\right) = 0, \\ F_{mat_{max}}, & \left(\dfrac{S_{wet_{wing}}}{S_{wet_{total}}}\right) = 1, \end{cases} \tag{18}$$

where $F_{mat_{max}}$ is the maximum possible material cost gain factor (as mentioned earlier, the factor ranges from 2.0 to 3.0). Solving Eq. 18, the material gain factor between 1.33 and 1.66 is obtained.

Table 7 Complexity gain factors for development costs.

Technology combination	Factor range
BWD-swept composite low-wing	1.40 - 1.60
FWD-swept composite mid-wing	1.50 - 1.70
FWD-swept composite low-wing	1.55 - 1.75
FWD-swept composite low-wing + over-the-wing engines	1.60 - 1.80

Finally, the aircraft unit price to be compared against reference aircraft in the market is defined by

$$P_{unit} = \frac{C_{RDTE} + C_{ACQ}}{N_{prog}} \tag{19}$$

where N_{prog} is the expected number of aircraft developed during the program. Existing information about annual sales for various business jet models was obtained from Ref. [51] and an average annual sale for each reference aircraft was extracted. In addition, three test aircraft were added during the development program. The production program of ten years was assumed.

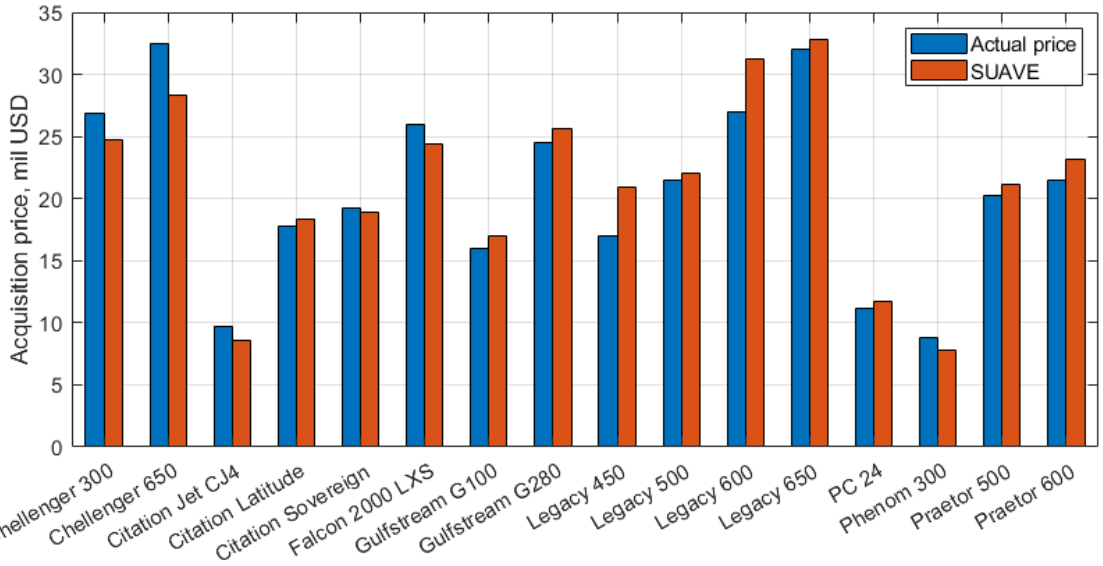

Fig. 7 Comparison between SUAVE-estimated aircraft prices and prices from the database for reference aircraft.

To ensure sufficient accuracy of the Roskam's development costs model, several database aircraft prices were estimated and compared against existing database information. Price estimates of selected business jets were obtained from the 'Air.one' online database, which includes either actual jet prices recommended by the manufacturer or the price estimate using internal models [30]. The comparison between SUAVE-modeled prices and reference values is presented in Figure 7. Obtained results demonstrated a satisfactory distribution of errors. A relative error for most aircraft does not exceed 15%, with the majority of them having an error of less than 10%. However, two aircraft out of sixteen demonstrated errors between 15% and 16%, and one aircraft had an error of 23%. The average difference between SUAVE and reference absolute prices for all sixteen aircraft is equal to 8.8%. Given the obtained, sufficient accuracy for the model was reached to be used for preliminary studies.

VI. Aircraft sizing considerations

Multiple aspects of the initial sizing were considered to ensure sufficient accuracy of model representation. For the fuselage, every aircraft features similar cabin dimensions to ensure the equivalent comparison between designed and

reference aircraft. Cabin dimensions were obtained from operating manuals, brochures, or cabin layouts available on the official websites of airplane manufacturers. Then, depending on the configuration, the remaining aircraft components are located according to the constraint analysis, MDO studies, and weights and balance assessments. Figure 8 demonstrates a sample layout of the super mid-size aircraft with a mid-located forward-swept wing where cabin components and areas indicated for fuel, systems, landing gear, and APU are represented. While aircraft with low-mounted wings and fuselage-mounted engines do not represent major changes from the original system's layout inside the fuselage, the mid-wing and aft-mounted engines layout involve additional design assumptions. For the mid-wing, extra fuselage length is required to fit the wing behind the pressure bulkhead. For both mid-size and super mid-size jets, an additional 0.75m was added to the fuselage length to fit the wing. For the light jet with wing-mounted engines, the original fuselage can be reduced since the volume required for the engine pylon becomes free. According to Nicolai [52], a similar configuration of a HondaJet managed to increase the fuselage volume by almost 20%. However, if the wing is swept forward, the wing root is located in the region where the baggage was located for the conventional aft-swept wing configuration. Consequently, if the cabin size is kept constant, the free space can now be used for the baggage compartment and the wing allocation to reduce the fuselage pressure drag. Due to the redistribution of components within the fuselage, no fuselage extension or reduction was assumed.

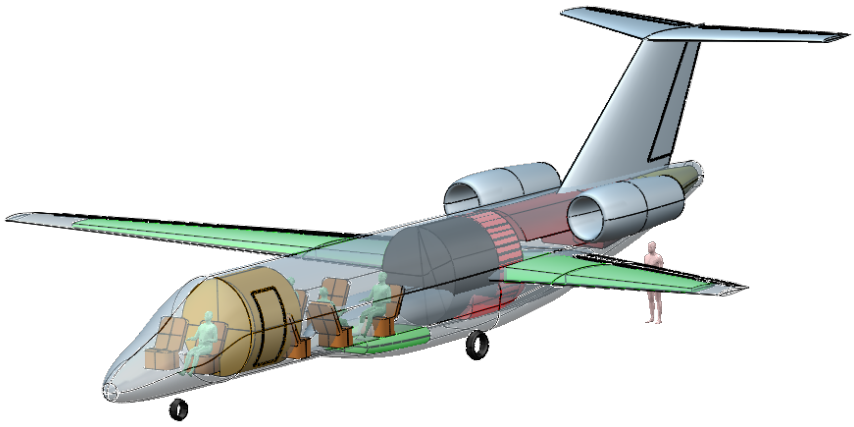

Fig. 8 Geometry of a super mid-size jet and its internal layout. Green areas represent fuel tanks, a golden section defines the galley, black segment shows the lavatory, red area defines the systems section, and yellow represents the APU.

The wing design assumptions play an important role in overall aircraft performance estimation and shall be treated carefully to ensure the capabilities of the wing are manufactured and maintained. Figure 9 shows a possible schematic layout of the wingbox and the example upper skin with spars and stringers manufactured during the LOMACHS project [53]. The leading edge skin can be manufactured using carbon fiber reinforced plastics (CFRP) with advanced anti-icing technologies or feature conventional anti-icing systems. The leading edge is mounted to the main wingbox with consists of the integral upper skin and the main spar part, the lower skin, and the rear spar. The lower skin is attached using

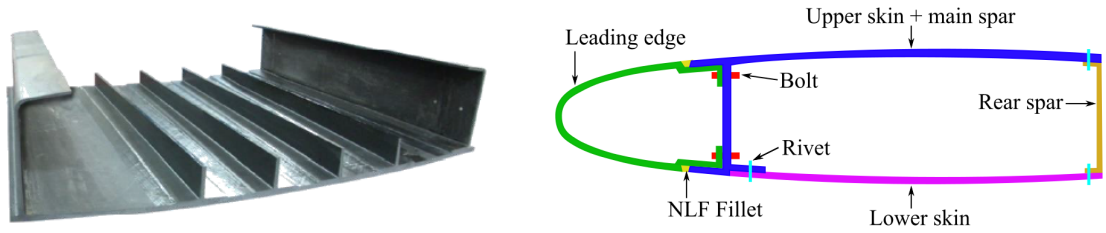

Fig. 9 A schematic structure of the wingbox featuring NLF and a sample manufactured upper skin. Adapted from [53].

flush rivets, which makes the wing easier to design and maintain since the lower skin can be unmounted to access the wingbox and work on internal systems. If flush rivets and an acceptable tolerance between the leading edge and the lower side skin is maintained, then NLF can be kept for both sides of the wing [54]. Both upper and lower skin feature smooth fillets, so sufficient smoothness can be achieved, and the NLF can be extended on both sides for as long as possible. Finally, the leading edge is bolted to the main spar and can be replaced by accessing the wingbox from the lower wing side. Due to the application of composite structures, wing weight reduction assumptions must be implemented. According to Raymer [36], up to 15% of the wing weight with respect to metallic structures can be reduced if advanced composites are implemented. For conventional backward-swept wings, a more conservative assumption of 10% reduction was used. For forward-swept wings, Kruse demonstrated a potential reduction of the wing weight by 8% compared to a conventional aluminum wing [55]. To maintain conservatism in the design due to limited research on forward-swept wings weight estimation, an assumption of no weight change of a forward-swept wing with respect to a backward-swept aluminum wing was implemented.

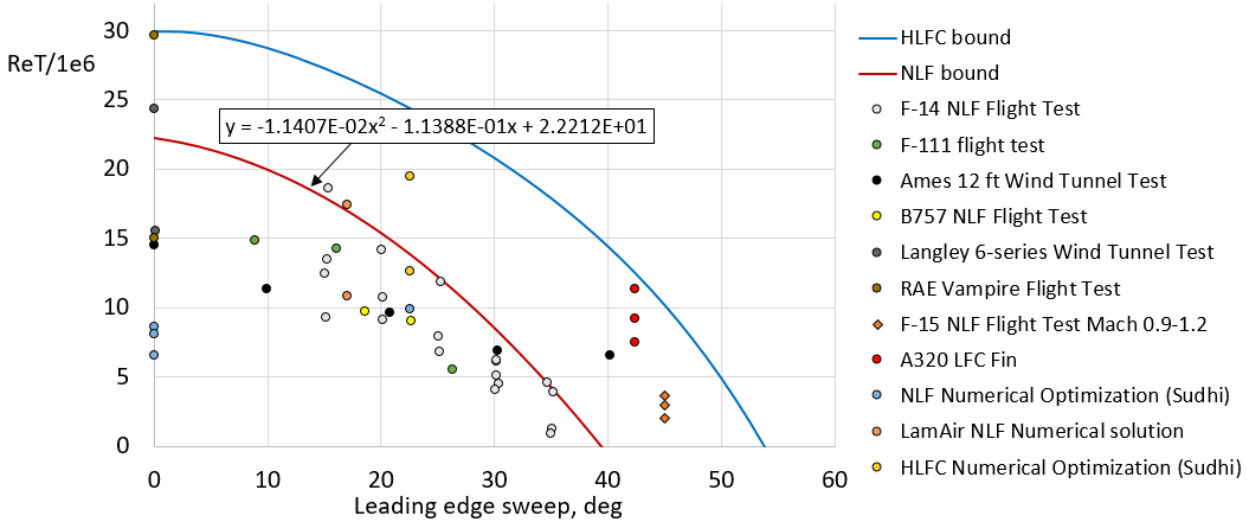

Fig. 10 Boundaries of NLF and HLF as a function of the leading edge sweep (ϕ_{LE}) and transition Reynolds number (Re_T) with experimental data . Derived from [56].

The transition model for the wing is based on the survey of Hepperle, who combined multiple experimental and numerical studies of NLF transition Reynolds number as a function of the wing sweep. Although such a model is simplistic and does not include details regarding the type of the airfoil and some specific operating and design considerations, it can be used for the initial estimates to study selected aircraft concepts with an actual design of wing with NLF. The maximum possible transition of 60% of the chord length was used based on studies of Seitz, who showed the transition location at 60% chord for the forward-swept mid-range aircraft, which corresponded to the location of the shock wave [13]. Due to a low-fidelity approach of the laminar flow estimation and lo-fidelity methods used for lift and drag estimations, airfoil definitions are limited to their thicknesses. More detailed characteristics of airfoils create an analysis limitation related to high angle-of-attack performance. In the present work, the adverse effect of NLF on high angle-of-attack performance was neglected, but they shall be addressed during the next design stage, where airfoil design and analysis will be performed.

Table 8 Summary of assumption considered for each designed aircraft.

Aircraft	**Wing weight gain**	**Fuselage extension**	**Boundary layer transition**	**Engine inter-ce drag**
All aircraft with BWD-swept wing	-10%	-	Re_T regression	-
Light jet, FWD-swept wing, wing-mounted engines	-	-	Re_T regression	+0.1 factor
All aircraft with the low, FWD-swept wing	-	-	Re_T regression	-
Mid-size and Super mid-size jets, FWD-swept, mid-wing	-	+0.75 m	Re_T regression	-

All aircraft feature single-slotted flaps for low-speed operations, For forward-swept configurations, an inboard droop nose similar to the one used for the HFB 320 Hansa Jet [57] may be necessary to avoid blanking of the horizontal stabilizer at high angles-of-attack. However, a more optimistic assumption of a careful inboard wing design was made to avoid additional design conservatism.

The contribution of wing-mounted engines was assumed to have additional interference drag due to higher speeds experienced by the pylon mounted near the wing. The engine interference factor was increased by 0.1 to account for this potential effect.

Finally, the empennage, engine nacelles, and fuselage do not feature NLF, and their transition was assumed 10% for the empennage, 5% for nacelles, and 0% for the fuselage. Table 8 summarizes all critical assumptions considered for all aircraft.

VII. Sizing results and discussions

A. Sensitivity of the aircraft range to the empty weight gain

Before sizing each configuration, it is important to investigate how much the empty weight gain function affects the possible NLF business jet design range. Three different empty weight gain curve fits shown in Figure 5 were implemented into the initial sizing block shown in Figure 4. The initial sizing trade study based on the wing loading for the minimum thrust-to-weight ratio was performed to estimate the design point with the maximum possible range extension for a given configuration. The wing aspect and taper ratios were fixed, and the values were similar to reference aircraft of each market segment. For the present study, only backward-swept configurations with corresponding design assumptions summarized in Table 8 were considered. Figure 11 summarizes the sensitivity study where upper and lower bounds represent the percent difference between the least-squares curve fit and corresponding bounds.

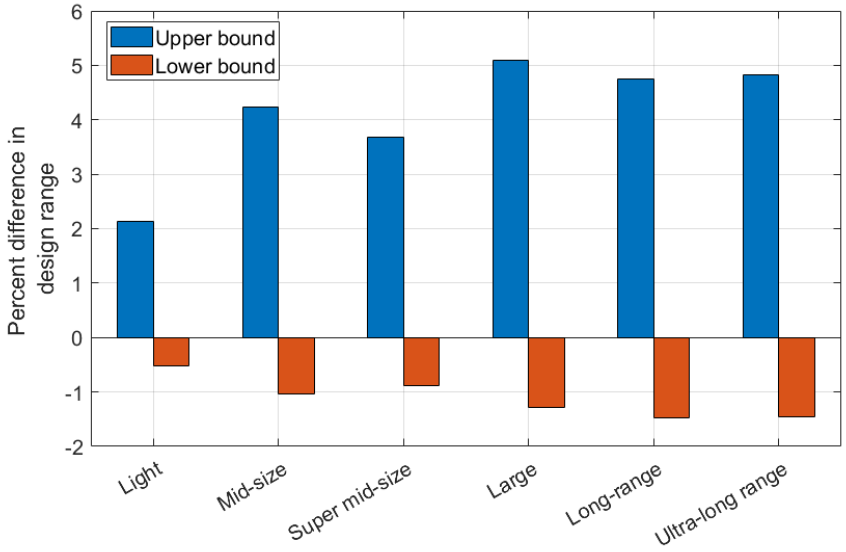

Fig. 11 Difference between the least squares design range and the design range on upper and lower $\Delta W_e/W_e$ bounds for various market segments.

Results demonstrate a non-linear change in the possible design range with respect to the empty weight gain factor. Such behavior corresponds to a shift in the design point due to a change in the aircraft drag. Since the process is iterative and the constraint analysis depends on the SUAVE mission analysis aerodynamic output, deviations in empty weight affect the point of the minimum thrust-to-weight ratio, which then changes the overall range extension capability. Reduction in the empty weight gain forces the design point to shift towards a lower wing loading. The opposite situation happens for the increase in the empty weight gain, but the shift is not as pronounced. The maximum range deviation is equal to 5% and occurs for large jets. Given trend also shows that the least-squares line corresponds to a more optimistic result since the lower bound difference in range is not as pronounced as the upper one. Given that the study is meant to be a market exploration based on the technology, where a moderate level of optimism can be maintained, the

least-squares line can be used for the analysis. This way, if the optimistic scenario does not make the aircraft potentially attractive, then a more conservative approach will not make it batter.

B. Design summary and price discussions

Figures 12 and 13 demonstrate the boundary layer transition line estimates for each designed aircraft configuration after their sizing and refinements using MDO.

Observing the boundary layer transition data, multiple trends are obtained. For light jets, both transition lines reach a maximum allowable chord ratio of due to the relatively low operational Reynolds number. For mid-size and super mid-size jets, aft-swept wings show earlier root transition due to a higher leading-edge sweep and Reynolds number and achievement of 60% laminar boundary layer at the mid-span. Starting from the super mid-size category, forward-swept wings also start demonstrating earlier root transition compared to smaller business jet categories. Since the mid-wing configuration assumed no droop nose at the root, the boundary layer transition profile was similar to the low-wing configuration. Finally, the boundary layer transition for long-range jets happens significantly earlier for the backward-swept configuration compared to large jets, which is an outcome of a higher wing sweep. However, the forward-swept configuration has the potential of maintaining laminar flow due to a relatively low sweep angle

Figure 14 compares reference and designed aircraft planforms, while Tables 9-23 in Appendix summarize sizing and MDO results for each designed aircraft configuration and compare configurations to reference configurations modeled in SUAVE. For all designed aircraft, the application of NLF enables aircraft to increase their aspect ratio to reduce the induced drag since the platform is not as sensitive to the parasite drag as it was before. The highest aspect ratio increase was observed for light and long-range jets because of more relaxed span constraints, while relatively small changes in aspect ratios were observed for other configurations. At the same time thickness of each wing almost always approached minimum values to reduce the compressibility drag. Along with the increase in aspect ratio, the planform area also increased, so aircraft are flown at lower wing loadings and require less engine thrust.

Due to the application of NLF technologies and the design goal to maintain a constant DOC, the distribution of costs changes with respect to the reference aircraft. The application of NLF reduces fuel consumption but increases maintenance costs. Consequently, the increase in maintenance costs limits the possibility of the aircraft maximizing its range. Figure 15 shows payload-range diagrams for five configurations with respect to their references after the sizing and refinement using MDO. aircraft configurations from light to Large jets could increase their range by 22-30% with respect to reference configurations, depending on the configuration. However, the long-range backward-swept jet could not reach similar values since the wetted area magnitude became significantly larger and increased maintenance cost stronger, while a substantial boundary layer extension due to a large wing sweep is unlikely to be achieved. At the same time, the forward-swept configuration demonstrated a range extension with respect to the reference aircraft, but it could not exceed 13% due to higher costs. Therefore, only one long-range configuration can be considered for the present

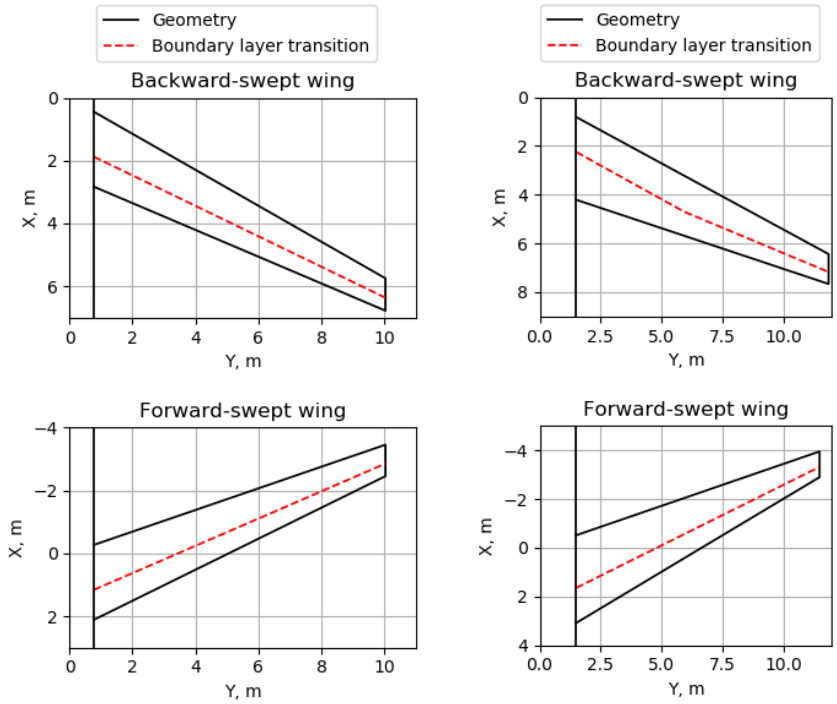

(a) Light jets boundary layer transition

(b) Large jets boundary layer transition

Fig. 12 Boundary layer transition profiles for light and large NLF aircraft.

study.

The aircraft range depends not only on the boundary layer transition profile but also on weight reduction assumptions and additional drag penalties for each configuration. In addition, assumptions affect maximum aircraft ranges for similar values of DOC. The combination of all these considerations results in a unique aircraft ranking with respect to particular parameters. Generally, the backward-swept configuration shows a slightly higher range due to the possibility to laminarize the flow and have additional weight reductions due to the application of composite materials. Forward-swept configurations have higher empty weights due to the assumption of the forward-swept wing divergence mitigation. Finally, the forward-swept mid-wing configurations have the highest empty weights due to longer fuselages, although the pressure drag of the fuselage was reduced.

To validate SUAVE results, a single point for each backward-swept NLF configuration was compared against the range estimation using the Breguet range equation. SUAVE payload-range diagram generation is based on the detailed mission analysis and calculation of each aircraft state at multiple time steps along the flight. Force-balance equations are used to determine the aircraft's attitude and required thrust to maintain the desired flight. Required thrust is compared to the physics-based engine model of Cantwell [45], whose parameters are defined by the designer. Finally, the fuel burn is obtained at each time step, and the range is dynamically extended or reduced depending on prescribed aircraft masses. Comparison of SUAVE and Breguet range equation results shows acceptable similarity. If all configurations

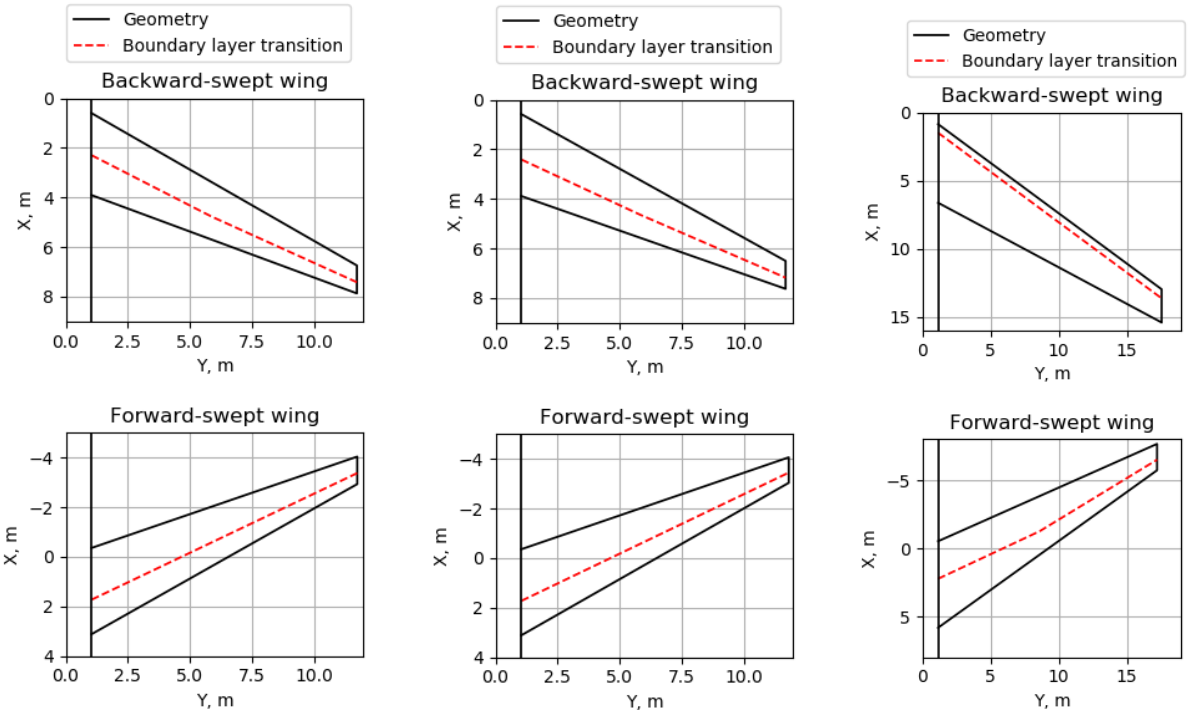

(a) Mid-size jets boundary layer transition

(b) Super mid-size jets boundary layer transition

(c) Large jets boundary layer transition

Fig. 13 Boundary layer transition profiles for mid-size and super mid-size NLF aircraft. The forward-swept mid-wing configurations features a similar boundary layer profile to the low-wing one.

are compared to their references, the designed flight distance extension ranges from 13% to 30% depending on the configuration.

Finally, the aircraft acquisition price for each NLF jet is presented in Figure 16. Colored circles on the PI chart represent initially bounded business jet market areas, and designed aircraft were plotted with existing aircraft to create specific ranges of potential PI indices and prices for each NLF aircraft group. Moreover, each aircraft price was represented as a range of values depending on technology and material cost assumptions. A more direct assessment of the aircraft price with respect to their reference aircraft and average market values is presented in Figure 17.

For light aircraft, the introduction of NLF leads to a minor increase in aircraft productivity compared to its reference to relatively low overall values of PI indices and lower contribution of the range as the PI index driver compared to other market segments. The price of NLF light jets increased by approximately 20% with respect to both reference and market values and became one of the more expensive jets in the category. However, due to a generally large production volume of aircraft similar to Embraer Phenom 300, production cost gains are redistributed such that the absolute price increase is not substantial. Observing the mid-size category, NLF aircraft demonstrate a significant increase in productivity due to the range extension and its influence on the PI index. Moreover, the increase in range moved the mid-size jet into the super mid-size category with respect to the PI index. However, technology and material cost penalties significantly

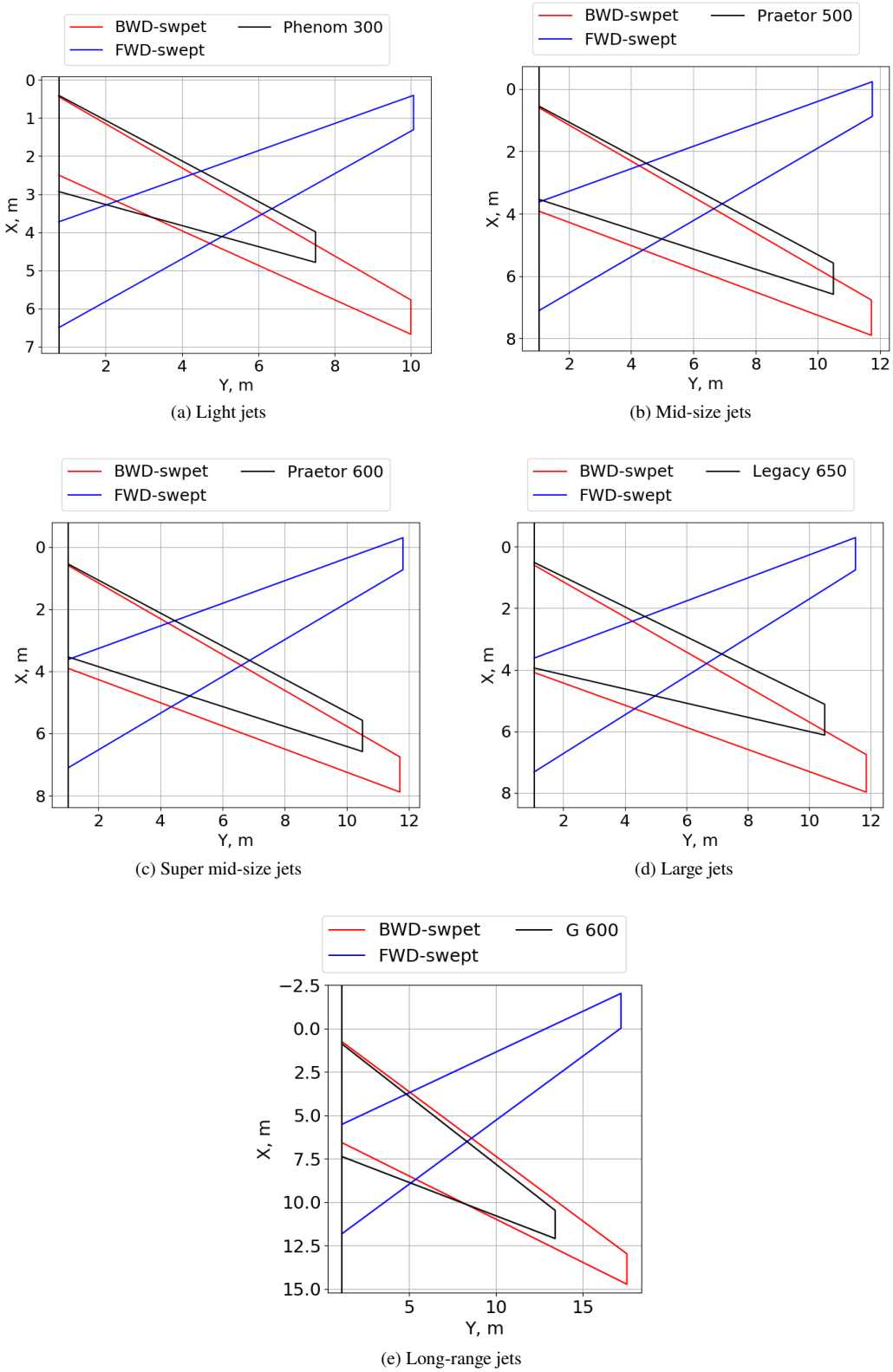

Fig. 14 Comparison of rectangular planforms between reference and designed aircraft.

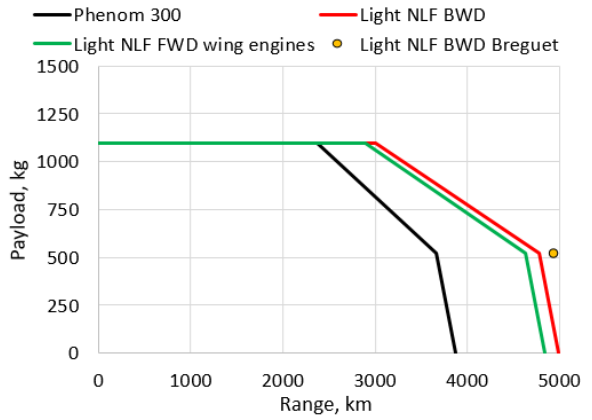

(a) Light jets

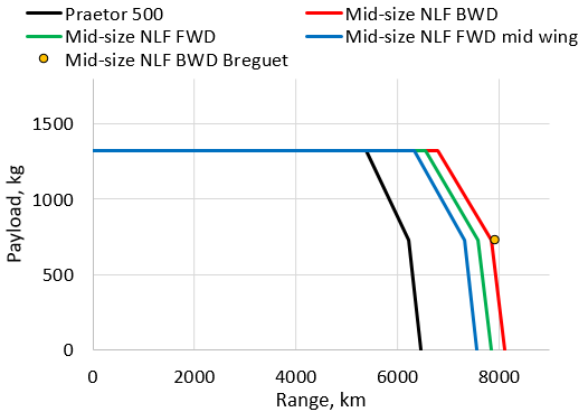

(b) Mid-size jets

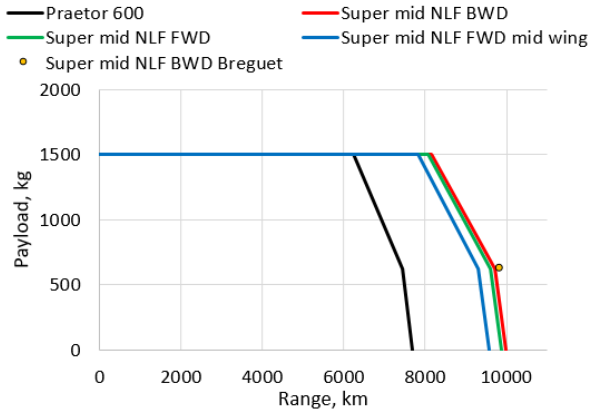

(c) Super mid-size jets

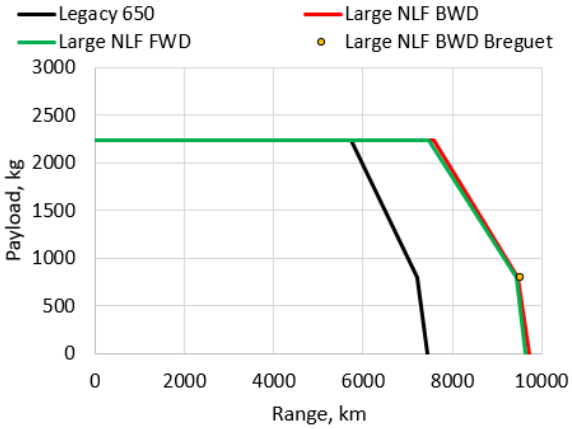

(d) Large jets

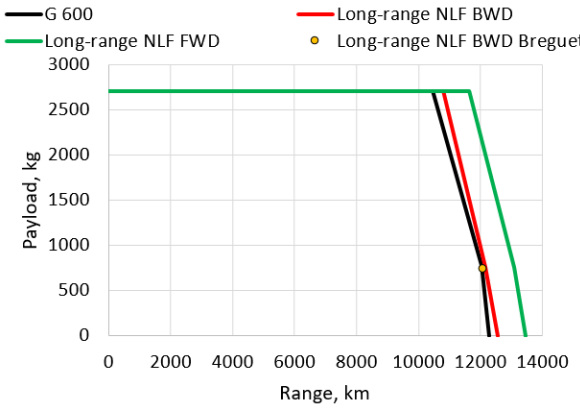

(e) Long-range jets

Fig. 15 Payload-range diagrams of designed aircraft.

increase the aircraft prices, moving them to higher price ranges. The backward-swept configuration shows the lowest possible price due to the lower empty weight, which is the major driver of the Roskam development costs model. The change in price with respect to both the reference and market average values is around 60%. The super mid-size category

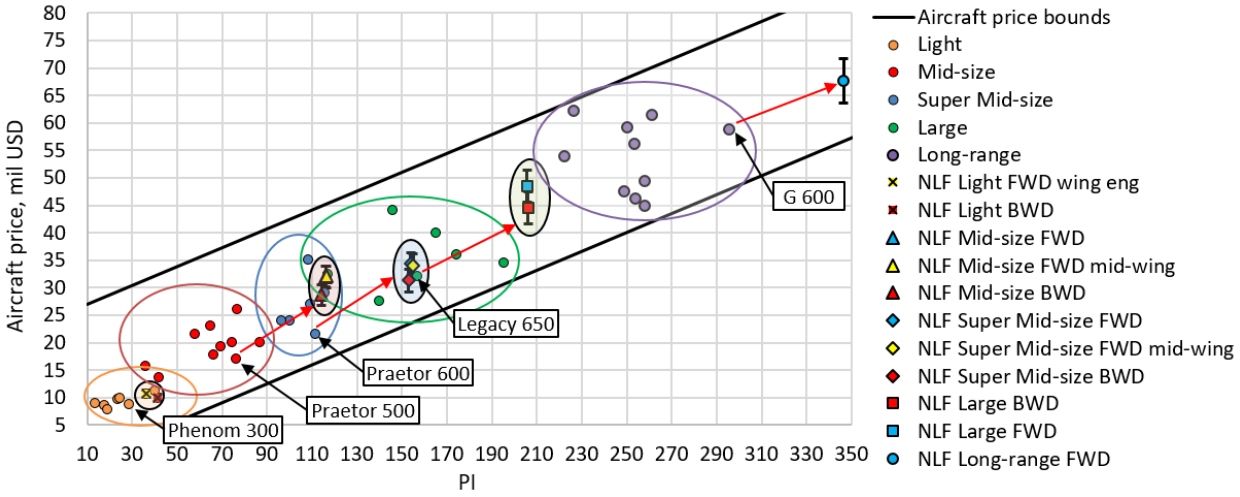

Fig. 16 Productivity Indices versus Prices for designed aircraft.

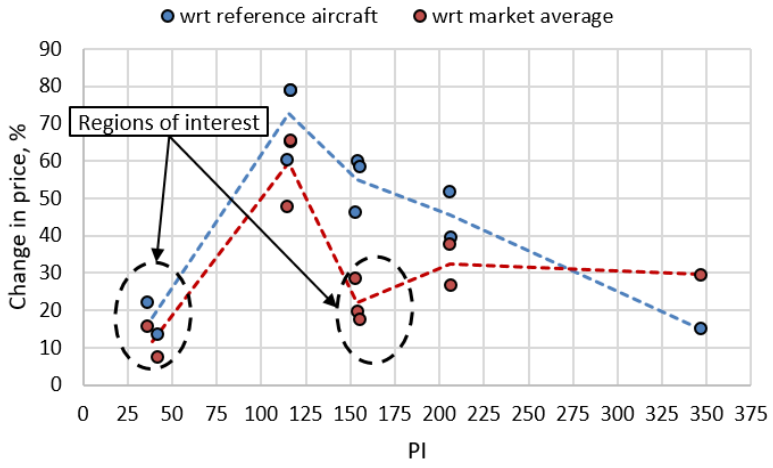

Fig. 17 Comparison of NLF aircraft prices with respect to reference aircraft and market average prices.

demonstrates the strongest increase in the PI index compared to all other segments. In addition, due to the reference configuration with a significant range extension, the NLF configuration also achieved the largest increase in range. Similar to the mid-size category, these aircraft have moved to the large category from the productivity perspective. The price has also increased by 55% with respect to the Praetor 600. However, according to the database, this aircraft has the lowest price in the market. If NLF jets are compared against market-average values, an increase in 20% is observed, making this jet close to the medium price range in the category and potentially interesting for customers due to the maximum range of around 9694 km (34% larger than the reference aircraft) and operating costs of the Praetor 600. For large jets, the range extension had a similar impact and magnitude to super mid-size jets. However, since the reference aircraft price is larger, the effect of price gains is stronger. While the backward-swept configuration is located closer to the middle of the price bounds, the forward-swept configuration demonstrates higher prices with similar performance. The change in price with respect to the reference aircraft is equal to 45%. If prices are compared to the market average,

the price increases by 31% for the backward-swept. Finally, the long-range forward-swept jet had a 30% increase in price with respect to the market average. Based on price sensitivities, the light and the super mid-size segments could potentially be beneficial due to their relatively moderate price gain with respect to the market.

To fully investigate aircraft economic impact of NLF technologies, total costs over a period of time for a fixed number of flight hours shall be investigated. The reason of including the aircraft price in the estimation of the total costs is motivated by a rather quickly [58], so it is important to not only have better operating costs but also not to have a significantly higher acquisition price, to have saved money (in case of private owners) or to start making profit quicker (in case of charter airlines). For charter airlines, fast depreciation rates help reduce the tax load in the long term. However, if the aircraft is generally cheaper, then the taxation rates will also be lower, which is also a benefit. To study the effect of total costs over time, two aircraft are compared for each segment. The designed NLF aircraft and the derivative of the reference aircraft with its range extended to the value of the NLF configuration. All geometric characteristics, as well as design wing loading and thrust-to-weight ratio, were kept constant for the extended reference aircraft. For the NLF option, a more optimistic lower bound of the development difficulty factor of 1.2 (compared to the baseline of 1.5 and 1.7 for aluminum aircraft) was considered as a bound of a virtual case when the technology becomes almost widely used and well-studied the aircraft segment. The material factor of 1.33 for development costs was taken as an optimistic scenario of material cost improvements. Finally, a higher operating rate of 750 hours per year was considered as a scenario of charter airline utilization.

Figure 18 summarizes total costs comparisons among prescribed aircraft in each market segment. Solid red lines represent NLF aircraft costs with baseline assumptions considered for the design, while error bars represent cost reduction due to potential technology maturity. Green lines present reference aircraft with a range extension to match the NLF aircraft range as an easier alternative to improve the aircraft PI. For the light jet segment, a potential matching of costs appears in approximately twelve years, which is a large period of time in the aircraft operating history. A similar situation is observed for mid-size jets, where the acquisition price was significantly higher than the reference aircraft. A more optimistic outcome was obtained for super mid-size and large jets, where the balance of the cost was achieved within ten and eight years, respectively. Such behavior was caused by a combination of not an excessive price increase and an improved airframe efficiency, which caused a reduction in operating costs per hour. Finally, the long-range aircraft price was substantially higher than the reference aircraft price, so the cost match was obtained at the year fourteen. Such results demonstrate that the costs of technologies could be a major obstacle for the business jet market, which does not have a high utilization compared to commercial aircraft. If the aircraft price effect cannot be mitigated by selling the aircraft at a relatively high price or the price is not reduced from the beginning via the reduction of development costs, the implementation of the technology is likely to be economically risky.

As mentioned previously, relatively low utilization of business jets significantly reduces the effectiveness of NLF applied to the aircraft. However, it is useful to know how quickly the cost balance can be achieved if the aircraft is flown

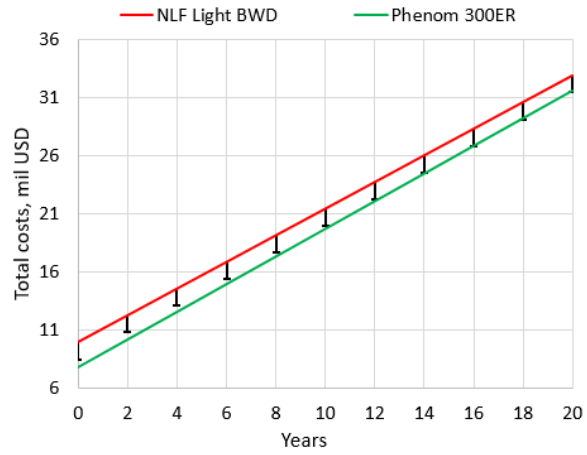

(a) Light jets

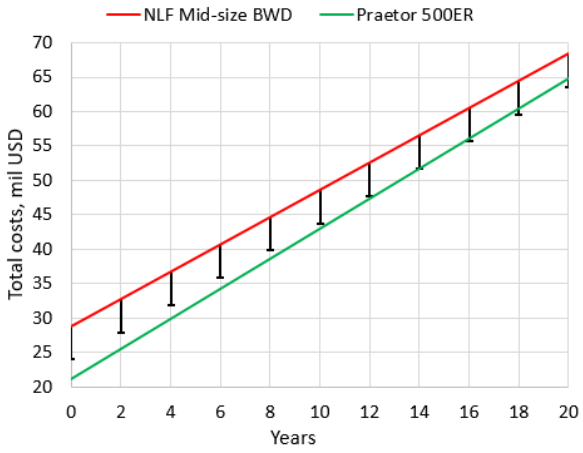

(b) Mid-size jets

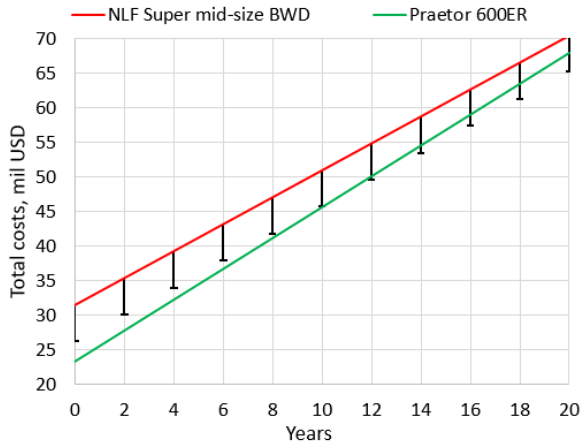

(c) Super mid-size jets

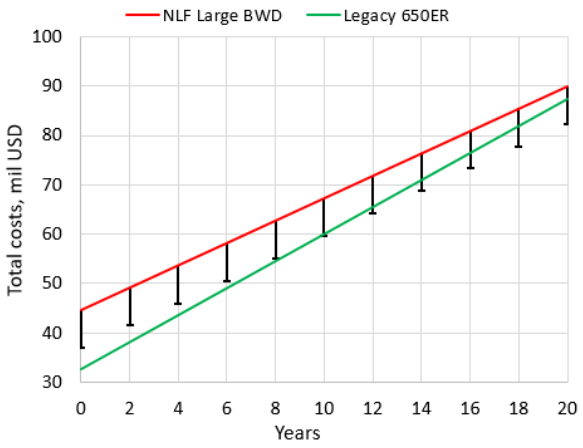

(d) Large jets

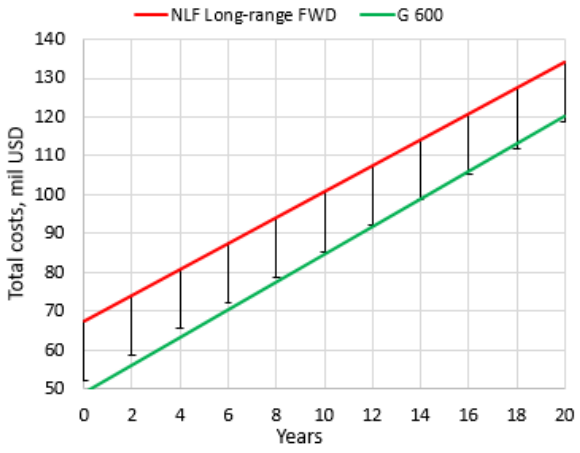

(e) Long-range jets

Fig. 18 Operating costs comparison for reference, extended reference, and designed aircraft for 750 flight hours/year.

for more hours. Figure 19 summarizes the sensitivity study of the super mid-size jet break-even point with respect to the extended-range reference aircraft to the number of flight hours per year.

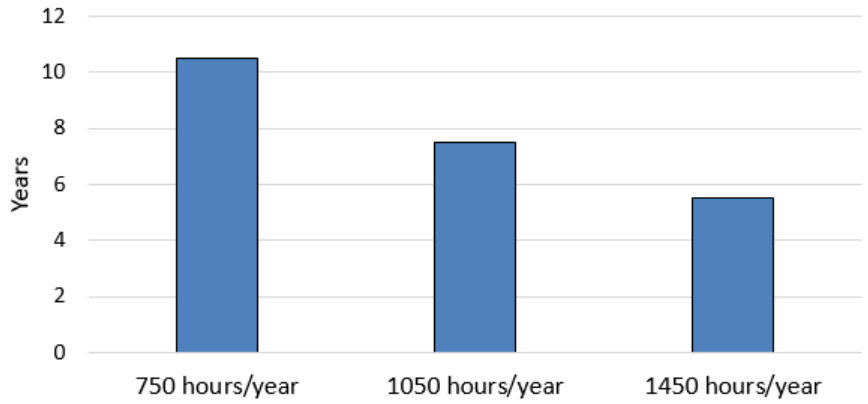

Fig. 19 Sensitivity study of the break-even costs point with respect to the reference extended-range reference aircraft as a function of operating flight hours.

Results of the sensitivity study show that if the number of flight hours is almost doubled compared to the reference value of 750 hours per year, the number of years required to match the total costs of the reference extended-range aircraft could reduce from ten years to almost five, which could be a more favorable operating scenario. If the aircraft acquisition price is reduced, then the trend will be even more pronounced, and the cost balance will occur even earlier.

VIII. Conclusion

The present work investigated the potential market applicability of natural laminar flow technologies for business jets. To perform the assessment, a database of 46 existing business jets has been generated to answer the question of what parameters of the PI index show the highest sensitivity for each market segment, from light to ultra long-range jets. The regression analysis indicated that the range extension generally plays a major role, so its increase is a strong market driver. This outcome motivated us to investigate how much NLF can extend an aircraft range without an increase in Direct Operating costs per year.

To quantify the potential of NLF aircraft, multiple configurations for each market segment have been sized. SUAVE initial sizing and MDO capabilities were used to size various aircraft configurations for each market. The SUAVE-embedded weights estimation method of FLOPS was calibrated to improve the weight estimation accuracy and assess model uncertainties. DOC and price estimation methods were validated to ensure adequate estimations for designed aircraft. In addition, aircraft acquisition prices with an account of technological and material complexities factors were obtained. Results demonstrated that the long-range backward-swept configuration was not able to substantially extend the aircraft range due to the combination of low laminarization and a significant increase in operating costs. For the remaining market segments, the range extension is between 13% and 30% depending on the aircraft configuration and

the market segment. Due to the implementation of NLF, acquisition prices for each aircraft increased. The least price growth was demonstrated by the backward-swept configuration due to the combination of NLF and weight reduction using composite materials for the wing. Based on obtained designs and costs analysis, super mid-size jets and large jets showed the best combinations of airframe efficiency improvements and acquisition price increases that enable the shortest possible costs break-even duration compared to reference aircraft. Other market segments have significant increases in development costs and insufficient improvements in operating costs to compensate for higher aircraft prices. However, even super mid-size and large jets require a substantial increase in operating flight hours to fully utilize the benefits of the NLF technology if present development and material costs are assumed. Alternatively, the reduction in costs shall be rather significant to fully utilize the benefits of the technology.

Finally, several questions remain open. First, a high level of uncertainty due to development complexities assumptions and material costs remain and must be assessed separately to ensure prediction accuracy and draw more accurate conclusions. Moreover, an implementation of detailed simulation models of the boundary layer over the wing and a direct design of airfoil section and wings for each aircraft would help determine a more certain range of the wing laminarization and improve the sizing process to lead to a more accurate result. Future work will focus on answering those questions to further improve the prediction methodology and increase the accuracy of current findings.

Appendix

Table 9 Geometric characteristics of NLF light business jets modeled in SUAVE.

Parameter	Light BWD-swept	Light BWD-swept wing engines	Phenom 300	Units
Wing				
Aspect ratio	11.4	11.5	8.5	-
Span	20.0	20.0	16.2	m
Taper ratio	0.4	0.4	0.33	-
Leading edge sweep	29.8	-20.0	24.8	deg
Dihedral	3.0	8.00	3.0	deg
Root thickness	0.11	0.11	0.13	
Tip thickness	0.10	0.09	0.1	
Horizontal tail				
Aspect ratio	4.3	4.16	4.1	-
Taper ratio	0.53	0.53	0.53	-
Leading edge sweep	30.0	30.0	30.0	deg
Thickness	0.09	0.09	0.09	
Vertical tail				
Aspect ratio	1.00	1.00	0.92	-
Taper ratio	0.63	0.63	0.63	-
Leading edge sweep	45.0	45.0	45.0	deg
Thickness	0.09	0.09		0.09

Table 10 Designed light aircraft weights breakdown modeled in SUAVE.

Parameter	Light BWD-swept	Light BWD-swept wing engines	Phenom 300	Units
Maximum take-off weight	7378	7614	8146	kg
Operating empty weight	4757	5002	5211	kg
Maximum Payload	1096	1096	1096	kg

Table 11 Geometric characteristics of NLF mid-size business jets modeled in SUAVE.

Parameter	Mid-size BWD-swept	Mid-size FWD-swept	Praetor 500	Units
Wing				
Aspect ratio	10.1	9.75	9.5	-
Span	22.5	23.5	21.4	m
Taper ratio	0.32	0.3	0.3	-
Leading edge sweep	30.0	-20.0	26.5	deg
Dihedral	3.0	8.00	3.00	deg
Root thickness	0.11	0.11	0.13	
Tip thickness	0.09	0.09	0.09	
Horizontal tail				
Aspect ratio	5.44	5.30	4.86	-
Taper ratio	0.60	0.60	0.58	-
Leading edge sweep	28.0	28.0	28.0	deg
Thickness	0.09	0.09	0.09	
Vertical tail				
Aspect ratio	1.13	1.13	1.04	-
Taper ratio	0.54	0.54	0.56	-
Leading edge sweep	45.0	45.0	45.0	deg
Thickness	0.09	0.09	0.09	

Table 12 Designed mid-size aircraft weights breakdown modeled in SUAVE.

Parameter	Mid-size BWD-swept	Mid-size FWD-swept	Mid-size FWD-swept mid-wing	Praetor 500	Units
Maximum take-off weight	16494	16937	17244	17030	kg
Operating empty weight	10037	10554	10843	10394	kg
Maximum Payload	1325	1325	1325	1325	kg

Table 13 Geometric characteristics of NLF super mid-size business jets modeled in SUAVE.

Parameter	Super mid-size BWD-swept	Super mid-size FWD-swept	Praetor 600	Units
Wing				
Aspect ratio	10.1	9.95	9.5	-
Span	23.4	23.6	21.4	m
Taper ratio	0.32	0.28	0.3	-
Leading edge sweep	30.0	-20.0	26.5	deg
Dihedral	3.0	8.00	3.0	deg
Root thickness	0.11	0.12	0.13	
Tip thickness	0.10	0.09	0.09	
Horizontal tail				
Aspect ratio	5.41	5.41	4.86	-
Taper ratio	0.50	0.50	0.57	-
Leading edge sweep	28.0	28.0	28.0	deg
Thickness	0.09	0.09	0.09	
Vertical tail				
Aspect ratio	1.13	1.13	1.04	-
Taper ratio	0.54	0.54	0.56	-
Leading edge sweep	45.0	45.0	45.0	deg
Thickness	0.09	0.09	0.09	

Table 14 Designed super mid-size aircraft weights breakdown modeled in SUAVE.

Parameter	Super mid-size BWD-swept	Super mid-size FWD-swept	Super mid-size FWD-swept mid-wing	Praetor 600	Units
Maximum take-off weight	17207	17452	17701	19346	kg
Operating empty weight	9588	9879	10132	11469	kg
Maximum Payload	1497	1497	1497	1497	kg

Table 15 Designed Large aircraft weights breakdown modeled in SUAVE.

Parameter	Large BWD-swept	Large FWD-swept	Legacy 650	Units
Maximum take-off weight	23628	23763	24325	kg
Operating empty weight	13685	13860	14160	kg
Maximum Payload	2240	2240	2240	kg

Table 16 Geometric characteristics of NLF Large business jets modeled in SUAVE.

Parameter	Large BWD-swept	Large FWD-swept	Legacy 650	Units
	Wing			
Aspect ratio	9.6	9.1	8.23	-
Span	23.7	23.0	20.6	m
Taper ratio	0.33	0.27	0.3	-
Leading edge sweep	30.0	-20.0	26.0	deg
Dihedral	3.0	6.0	3.0	deg
Root thickness	0.11	0.11	0.13	
Tip thickness	0.09	0.09	0.11	
	Horizontal tail			
Aspect ratio	4.6	4.6	4.8	-
Taper ratio	0.6	0.6	0.6	-
Leading edge sweep	22.0	22.0	22.0	deg
Thickness	0.09	0.09	0.09	
	Vertical tail			
Aspect ratio	1.25	1.27	1.21	-
Taper ratio	0.56	0.56	0.56	-
Leading edge sweep	35.0	35.0	35.0	deg
Thickness	0.09	0.09	0.09	

Table 17 Designed Long-range aircraft weights breakdown modeled in SUAVE.

Parameter	Long-range BWD-swept	Long-range FWD-swept	G 600	Units
Maximum take-off weight	43405	44096	43182	kg
Operating empty weight	23300	24467	22959	kg
Maximum Payload	2708	2708	2708	kg

Table 18 Geometric characteristics of NLF Long-range business jets modeled in SUAVE.

Parameter	Long-range BWD-swept	Long-range FWD-swept	G600	Units
	Wing			
Aspect ratio	8.3	8.0	7.35	-
Span	31.2	32.5	29.0	m
Taper ratio	0.25	0.25	0.18	-
Leading edge sweep	40.0	-25.0	39.0	deg
Dihedral	2.0	6.0	2.0	deg
Root thickness	0.11	0.11	0.11	
Tip thickness	0.09	0.09	0.09	
	Horizontal tail			
Aspect ratio	4.8	5.0	4.7	-
Taper ratio	0.5	0.5	0.5	-
Leading edge sweep	35.0	35.0	35.0	deg
Thickness	0.09	0.09	0.09	
	Vertical tail			
Aspect ratio	1.05	1.08	1.04	-
Taper ratio	0.64	0.64	0.64	-
Leading edge sweep	40.0	40.0	40.0	deg
Thickness	0.09	0.09	0.09	

Table 19 Designed Light aircraft Performance characteristics modeled in SUAVE.

Parameter	Light BWD-swept	Light BWD-swept with wing engines	Phenom 300	Units
Range (4 PAX, max fuel)	4767	4616	3723	km
Takeoff field length	875	973	987	m
Landing distance	630	670	674	m

Table 20 Designed Mid-size aircraft Performance characteristics modeled in SUAVE.

Parameter	Mid-size BWD-swept	Mid-size FWD-swept	Mid-size FWD-swept mid-wing	Praetor 500	Units
Range (4 PAX, max fuel)	7827	7571	7303	6186	km
Takeoff field length	1240	1186	1185	1287	m
Landing distance	598	572	579	636	m

Table 21 Designed Super mid-size aircraft Performance characteristics modeled in SUAVE.

Parameter	Super mid-size BWD-swept	Super mid-size FWD-swept	Super mid-size FWD-swept mid-wing	Phraetor 600	Units
Range (4 PAX, max fuel)	9694	9590	9298	7441	km
Takeoff field length	1286	1265	1270	1352	m
Landing distance	654	647	650	692	m

Table 22 Designed Large aircraft Performance characteristics modeled in SUAVE.

Parameter	Large BWD-swept	Large FWD-swept	Legacy 650	Units
Range (4 PAX, max fuel)	9472	9445	7223	km
Takeoff field length	1745	1750	1750	m
Landing distance	857	860	866	kg

Table 23 Designed Long-range aircraft Performance characteristics modeled in SUAVE.

Parameter	Long-range BWD-swept	Long-range FWD-swept	G 600	Units
Range (8 PAX, max fuel)	12150	13100	12040	km
Takeoff field length	1625	1670	1737	m
Landing distance	895	910	945	kg

Acknowledgments

We would like to acknowledge the funding by the Deutsche Forschungsgemeinschaft (DFG, German Research Foundation) under Germany's Excellence Strategy—EXC 2163/1-Sustainable and Energy Efficient Aviation—Project-ID 390881007.

References

[1] Beck, N., Landa, T., Seitz, A., Boermans, L., Liu, Y., and Radespiel, R., "Drag Reduction by Laminar Flow Control," *Energies*, Vol. 11, No. 1, 2018. https://doi.org/10.3390/en11010252.

[2] Sudhi, A., Elham, A., and Badrya, C., "Coupled Boundary-Layer Suction and Airfoil Optimization for Hybrid Laminar Flow Control," *AIAA Journal*, Vol. 59, No. 12, 2021. https://doi.org/10.2514/1.J060480.

[3] Sudhi, A., Radespiel, R., and Badrya, C., "Design of Transonic Swept Wing for HLFC Application," *AIAA Aviation 2021 Forum*, August 2-6, 2021. https://doi.org/10.2514/6.2021-2606.

[4] Collazo Garcia III, A., and Ansell, P., "Characterization of a Griffith-Type Transonic, Laminar-Flow Airfoil," *Journal of Aircraft*, Vol. 56, No. 4, 2019. https://doi.org/10.2514/1.C035221.

[5] Schrauf, G., and von Geyr, H., "Hybrid Laminar Flow Control on A320 Fin: Retrofit Design and Sample Results," *Journal of Aircraft*, Vol. 58, No. 6, 2021. https://doi.org/10.2514/1.C036179.

[6] Risse, K., and Stumpf, E., "Conceptual Aircraft Design including Hybrid Laminar Flow Control," *CEAS Aeronaut. J*, , No. 5, 2014, pp. 333, 343. https://doi.org/10.1007/s13272-014-0111-6.

[7] Mosca, V., Karpuk, S., Badrya, C., and Elham, A., "Multidisciplinary design optimisation of a fully electric regional aircraft wing with active flow control technology," *Aeronautical Journal*, Vol. First view, 2021. https://doi.org/10.1017/aer.2021.101.

[8] Saeed, T., Graham, W., and Hall, C., "Boundary-Layer Suction System Design for Laminar-Flying-Wing Aircraft," *Journal of Aircraft*, Vol. 48, No. 4, 2011. https://doi.org/10.2514/1.C031283.

[9] Graham, W., and Saeed, T., "Design Study for a Laminar-Flying-Wing Aircraft," *Journal of Aircraft*, Vol. 52, No. 5, 2015. https://doi.org/10.2514/1.C032862.

[10] Pohya, A., Wicke, K., Risse, K., Linke, F., Lau, A., Lührs, B., and Swaid, M., "Cloud Encounter Impact on Operational and Economical Effectiveness of Hybrid-Laminar-Flow-Control Aircraft," *Journal of Aircraft*, Vol. 56, No. 4, 2019. https://doi.org/10.2514/1.C035205.

[11] Schrauf, G., and Geyr, H., "Simplified Hybrid Laminar Flow Control for the A320 Fin - Aerodynamic and System Design, First Results," *AIAA Scitech 2020 Forum*, 6-10 Jan 2020. https://doi.org/10.2514/6.2020-1536.

[12] Holmes, B., Obara, C., Martin, G., and Domack, C., "Manufacturing Tolerances for natural Laminar Flow Airframe Surfaces," *SAE Technical Paper 850863*, 1985. https://doi.org/10.4271/850863.

[13] Seitz, A., Hübner, A., and Risse, K., "The DLR TuLam project: design of a short and medium range transport aircraft with forward swept NLF wing," *CEAS Aeronautical Journal*, Vol. 2020, No. 11, 2020. https://doi.org/10.1007/s13272-019-00421-1.

[14] Xu, J., and Kroo, I., "Aircraft Design with Active Load Alleviation and Natural Laminar Flow," *Journal of Aircraft*, Vol. 51, No. 5, 2014. https://doi.org/10.2514/1.C032402.

[15] Fan, Z., Yu, X., Qin, N., and Zhu, M., "Benefit Assessment of Low-Sweep Transonic Natural Laminar Flow Wing for Commercial Aircraft," *Journal of Aircraft*, Vol. 58, No. 6, 2021. https://doi.org/10.2514/1.C036138.

[16] de Rosa, P., Mele, R., and Moens, F., "Performance Improvements of a Regional Aircraft by Riblets and Natural Laminar Flow," *Journal of Aircraft*, Vol. 57, No. 1, 2019. https://doi.org/10.2514/1.C035445.

[17] Lammering, T., Eckhard, A., Risse, K., Franza, K., and Hoernschemeryer, R., "Influence of Offdesign Performance on Design Synthesis of Laminar Aircraft," *Journal of Aircraft*, Vol. 49, No. 5, 2012. https://doi.org/10.2514/1.C031663.

[18] Wicke, K., Linke, F., Gollnick, V., and Kruse, M., "Insect Contamination Impact on Operational and Economic Effectiveness of Natural-Laminar-Flow Aircraft," *Journal of Aircraft*, Vol. 53, No. 1, 2015. https://doi.org/10.2514/1.C033237.

[19] Wunderlich, T., and Dähne, S., "Aeroelastic tailoring of an NLF forward swept wing: DLR contribution to LuFo IV joint research project AeroStruct," *CEAS Aeronautical Journal*, Vol. 8, No. 3, 2017. https://doi.org/10.1007/s13272-017-0251-6.

[20] Steffen, O., Buggisch, M., Kappel, E., Köke, H., Meyer, P., and Hühne, C., "Flight Testing on Ground - The Laminar Wing Leading Edge Ground Based Demonstrator," *Deutscher Luft- und Raumfahrtkongress DLRK 2019*, 30 Sept - 2 Oct 2019. URL https://elib.dlr.de/134022/.

[21] Steffen, O., Buggisch, M., Kappel, E., Köke, H., Meyer, P., and Hühne, C., "Flight Testing on Ground - The Laminar Wing Leading Edge Ground Based Demonstrator," *Deutscher Luft- und Raumfahrtkongress DLRK 2019*, 12 Sep - 2 Oct 2019. URL https://elib.dlr.de/134022/.

[22] Heinrich, L., and Kruse, M., "Laminar Composite Wing Surface Waviness - Two Counteracting Effects and a Combined Assessment by Two Methods," *Deutscher Luft- und Raumfahrtkongress 2016*, 13 - 15 Sept 2016. URL https://elib.dlr.de/118894/.

[23] Nangia, R., "Forward-swept wings and Application in High Aspect Ration Aircraft Configurations," *In Proceedings of Unconventional Aircraft Concepts Symposium*, 24 Apr 1987.

[24] Iuliano, E., Quagliarella, D., and Donell, R., "Design of a Supersonic Natural Laminar Flow Wing–Body," *Journal of Aircraft*, Vol. 48, No. 4, 2011. https://doi.org/10.2514/1.C031039.

[25] Quagliarella, D., and Iuliano, E., "Robust Design of a Supersonic Natural Laminar Flow Wing-Body," *Journal of Aircraft*, Vol. 12, No. 4, 2017. https://doi.org/10.1109/MCI.2017.2742718.

[26] Sturdza, P., "Extensive Supersonic Natural Laminar Flow on the Aerion Business Jet," *45th AIAA Aerospace Sciences Meeting and Exhibit*, 08 - 11 January 2007. https://doi.org/10.2514/6.2007-685.

[27] Somers, D., "Design of a Slotted, Natural-Laminar-Flow Airfoil for Business-Jet Applications," *CR–2012-217559*, 2012.

[28] Fujino, M., "Design and Development of the HondaJet," *Journal of Aircraft*, Vol. 42, No. 13, 2005. https://doi.org/10.2514/1.12268.

[29] Isikveren, A., Goritschnig, G., and Noel, M., "Productivity Metrics for Business and Regional Aircraft," *SAE 2003 Transactions Journal of Aerospace*, Vol. 112, No. 1, 2003. https://doi.org/10.4271/2003-01-3063.

[30] "Air.one, Online aircraft database," 2021. URL http://web.archive.org/web/20210826095413/https://air.one/.

[31] "Annex 6 to the Convention on International Civil Aviation, Operation of Aircraft, Part 1, International Commercial Air Transport - Aeroplanes," 2010. URL https://perma.cc/9HK6-6ZKX.

[32] "Certification Specifications and Acceptable Means of Compliance for Large Aeroplanes CS-25," 2020. URL www.easa.europa.eu/document-library/certification-specifications/cs-25-amendment-25.

[33] McDonald, R., "Design and Development of the HondaJet," *16th AIAA Aviation Technology, Integration, and Operations Conference*, 13-17 Jun 2016. https://doi.org/10.2514/6.2016-3282.

[34] Lukaczyk, T., Wendroff, A., Colonno, M., Economon, T., Alonso, J., and Orra, T., "SUAVE: An Open-Source Environment for Multi-Fidelity Conceptual Vehicle Design," *16th AIAA ISSMO Multidisciplinary Analysis and Optimization Conference*, 22-26 June 2015. https://doi.org/10.2514/6.2015-3087.

[35] Gudmundsson, S., *General Aviation Aircraft Design: Applied Methods and Procedures*, 1st ed., Butterworth-Heinemann, Oxford, UK, 2013.

[36] Raymer, D., *Aircraft Design: A Conceptual Approach*, 6th ed., American Institute of Aeronautics and Astronautics, Washington, DC, USA, 2018. https://doi.org/10.2514/4.104909.

[37] Torenbeek, E., *Synthesis of Subsonic Airplane Design*, Springer, Delft, Netherlands, 1982. https://doi.org/10.1007/978-94-017-3202-4.

[38] Roskam, J., *Airplane Design*, 2nd ed., Darcorporation, Lawrence, KS, USA, 2003.

[39] Hoelzen, J., Liu, Y., Bensmann, B., Winnefeld, C., Elham, A., Friedrichs, J., and Hanke-Rauschenbach, R., "Conceptual Design of Operation Strategies for Hybrid-Electric Aircraft," *Energies*, Vol. 11, No. 1, 2018. https://doi.org/10.3390/en11010217.

[40] Scholz, D., "Aircraft Design - an Open Educational Resource (OER) for Hamburg Open Online University (HOOU)," 2017. URL https://web.archive.org/web/20210716141759/https://www.fzt.haw-hamburg.de/pers/Scholz/HOOU/AircraftDesign_7_WingDesign.pdf.

[41] *Annex 14 to the Convention on International Civil Aviation, Aerodromes, Volume 1, 8th Edition*, July 2018.

[42] Andersson, J., and P. Krus., P., "A Multi-Objective Optimization Approach to Aircraft Preliminary Design," *SAE World Aviation Congress*, 8-11 Sept 2003. https://doi.org/10.4271/2003-01-3012.

[43] Wells, D., Horvath, B., and McCullers, L., "The Flight Optimization System Weights Estimation Method," *TM 20170005851*, Vol. 11, No. 1, 2017. URL https://core.ac.uk/display/84913944.

[44] Obert, E., *Aerodynamic Design of Transport Aircraft*, IOS Press BV, Netherlands, 2009.

[45] Cantwell, B., *Aircraft and Rocket Propulsion*, Stanford University, Stanford, CA, USA, 2022.

[46] Croom, C., and Holmes, B., "Flight Evaluation of an Insect Contamination Protection System for Laminar Flow Wings," *SAE Technical Paper 850860*, 1985. https://doi.org/10.4271/850860.

[47] Dutton, S., Kelly, D., and Baker, A., *Composite Materials for Aircraft Structures*, 2nd ed., American Institute of Aeronautics and Astronautics, Washington, DC, USA, 2012.

[48] "Glbal Air. Aviation fuel price statistics," 2021. URL https://web.archive.org/web/20210830131107/https://www.globalair.com/airport/region.aspx.

[49] Franz, K., "CeRAS Direct Operating Cost (DOC) Model; RWTH Aachen University," 2014. URL https://web.archive.org/web/20210830133810/http://ceras.ilr.rwth-aachen.de/trac/export/HEAD/CeRas/Downloads/Tools_and_Methodologies/DOCMethod_CeRAS_TUBerlin.pdf.

[50] "Compare Private Planes, Online aircraft database," 2021. URL http://web.archive.org/web/20210826094454/https://compareprivateplanes.com/.

[51] "General Aviation Manufacturers Association. Annual Report 2018," 2018. URL https://perma.cc/QC53-W2RJ.

[52] Carichner, G., and Nicolai, L., *Fundamentals of Aircraft and Airship Design, Volume 2 – Airship Design and Case Studies*, 2nd ed., American Institute of Aeronautics and Astronautics, Washington, DC, USA, 2013. https://doi.org/10.2514/4.868986.

[53] Weiland, M., "Low Cost Manufacturing and Assembly of Composite and Hybrid Structures," 2016. https://doi.org/https://web.archive.org/web/20210830233103/https://cordis.europa.eu/docs/results/314/314003/final1-locomachs-final-publishable-summary-report-r1-0.pdf.

[54] Holmes, B. J., and Obara, C. J., "Observations and implications of natural laminar flow on practical airplane surfaces," *Journal of Aircraft*, Vol. 20, No. 12, 1983, pp. 993–1006. https://doi.org/10.2514/3.48203.

[55] Kruse, M., Wunderlich, T., and Heinrich, L., "A Conceptual Study of a Transonic NLF Transport Aircraft with Forward Swept Wings," *30th AIAA Applied Aerodynamics Conference*, 25-28 Jun 2012. https://doi.org/10.2514/6.2012-3208.

[56] Hepperle, M., "MDO of Forward Swept Wings," *In Proceedings of the KATnet II Workshop*, 29-29 Jan 2008. URL https://perma.cc/SYY4-RVT9.

[57] "Sweptforward Wings for the HFB 320 Hansa: An Outline of the Design Considerations which Led to the Adoption of Sweptforward Wings for the Hamburger Flugzeugbau Hansa Jet Executive Aircraft," *Aircraft Engineering and Aerospace Technology*, Vol. 36, No. 8, 1964. https://doi.org/10.1108/eb033915.

[58] Hoover, J., "A Detailed Analysis of § 280F Depreciation Recapture for Business Aircraft," *National Business Aviation Association*, 2017.